

Discovery of Bis-imidazolecarboxamide Derivatives as Novel, Potent, and Selective TNIK Inhibitors for the Treatment of Idiopathic Pulmonary Fibrosis

Vladimir Aladinskiy,* Chris Kruse, Luoheng Qin, Eugene Babin, Yaya Fan, Georgiy Andreev, Heng Zhao, Yanyun Fu, Man Zhang, Yan Ivanenkov, Alex Aliper, Alex Zhavoronkov, and Feng Ren

Cite This: *J. Med. Chem.* 2024, 67, 19121–19142

Read Online

ACCESS |



Metrics & More

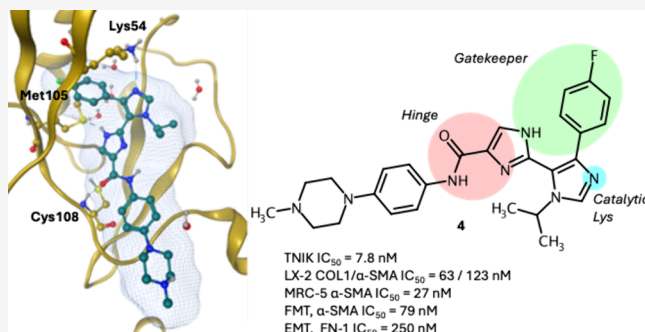


Article Recommendations



Supporting Information

ABSTRACT: Traf2- and Nck-interacting kinase (TNIK) has been identified as a promising therapeutic target for the treatment of fibrosis-driven diseases. Utilizing a structure-based drug design workflow, we developed a series of potent TNIK inhibitors that modulate the conformation of the gatekeeper Met105 side chain and access the TNIK back pocket. The lead optimization efforts culminated in the discovery of the recently reported compound 4 (INS018_055), a novel TNIK inhibitor. This molecule demonstrated excellent activity in both enzymatic and cell-based assays, along with high selectivity in a kinome panel. Further, *in vitro* and *in vivo* preclinical studies revealed favorable *in vitro* and *in vivo* DMPK properties. Results from multiple cell-based and animal models proved that compound 4 exhibits considerable antifibrotic and anti-inflammatory efficacy. Currently, phase II clinical trials of compound 4 are underway for the treatment of idiopathic pulmonary fibrosis (IPF).



INTRODUCTION

Traf2- and Nck-interacting kinase (TNIK) is a serine/threonine kinase and belongs to the germinal center kinases of the STE20 family. TNIK has been initially considered a potential target for the treatment of colorectal cancer (CRC)^{1–4} due to its direct involvement in Wnt signaling. More recently, targeting TNIK, particularly in combination with inhibiting cancer-related kinases, has also been reported as a suitable strategy for treating other cancers, such as lung squamous cell carcinoma (LSCC),^{5,6} triple-negative breast cancer (TNBC),⁷ ovarian cancer,⁸ thyroid cancer,^{9–11} and synovial sarcoma.¹²

Compounds 1, 2, and 3 are previously reported TNIK inhibitors evaluated in Wnt-active CRC cell lines (Figure 1). NCB-0846 (1) demonstrated TNIK inhibition with an IC_{50} of 21 nM and antiproliferative activity in HCT-116 cells both *in vitro* and *in vivo*.¹³ It was later reported that compound 1 is a multikinase inhibitor exhibiting anticancer potency in multiple cancer cell lines.¹⁴ Interestingly, tool compound 2 displayed micromolar activity against HCT-116 and DLD-1 (IC_{50} s of 2–6 μ M), despite exhibiting high inhibitory activity against TNIK (IC_{50} = 8 nM).¹⁵ Compound 3 is a nanomolar TNIK inhibitor (IC_{50} = 26 nM) with a more selective profile than that for compound 1.¹⁴ It also showed antiproliferative activity in HCT-116 and DLD-1 cells with IC_{50} values in a micromolar range (4–8 μ M). Despite recent advances in the development of TNIK inhibitors, there are no currently ongoing clinical trials for TNIK inhibitors in cancer indications.

Idiopathic pulmonary fibrosis (IPF) is a chronic, progressive, and fatal interstitial lung disease. Its main pathological characteristics include damage to alveolar epithelial cells, fibroblast activation, and extracellular matrix accumulation, which gradually lead to damage to the lung structure and decreased lung function.¹⁶ Despite the progress in treatment with FDA-approved antifibrotics, pirfenidone and nintedanib, IPF still remains a life-threatening condition with an unfavorable prognosis.¹⁷ In our recent work, we reported TNIK as a suitable target for lung fibrosis, identified with AI-driven methodologies,¹⁸ and demonstrated the efficacy of highly selective TNIK inhibitor INS018_055 (4) in multiple fibrosis and inflammation animal models.¹⁹ TNIK is involved in several critical signaling pathways, such as nuclear factor kappa B (NF- κ B), c-Jun N-terminal kinase (JNK), and Wnt, which are implicated in fibrosis. The NF- κ B pathway is a key player in the development of fibrosis in various organs, including the lungs.²⁰ TNIK's involvement in this pathway suggests that it could play a role in the fibrotic response seen in IPF.²¹ Similarly, the Wnt

Received: July 10, 2024

Revised: September 18, 2024

Accepted: September 26, 2024

Published: October 18, 2024



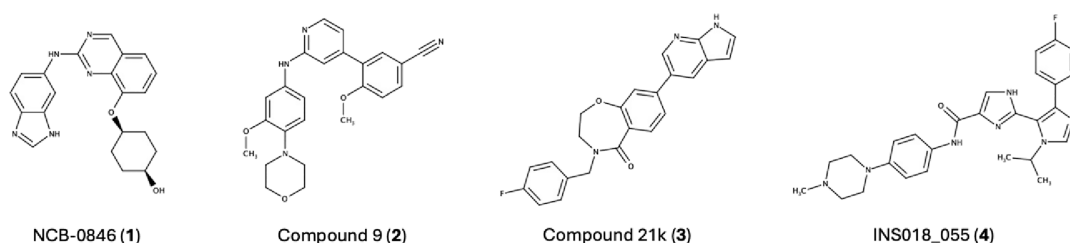


Figure 1. Chemical structures of known TNK inhibitors.

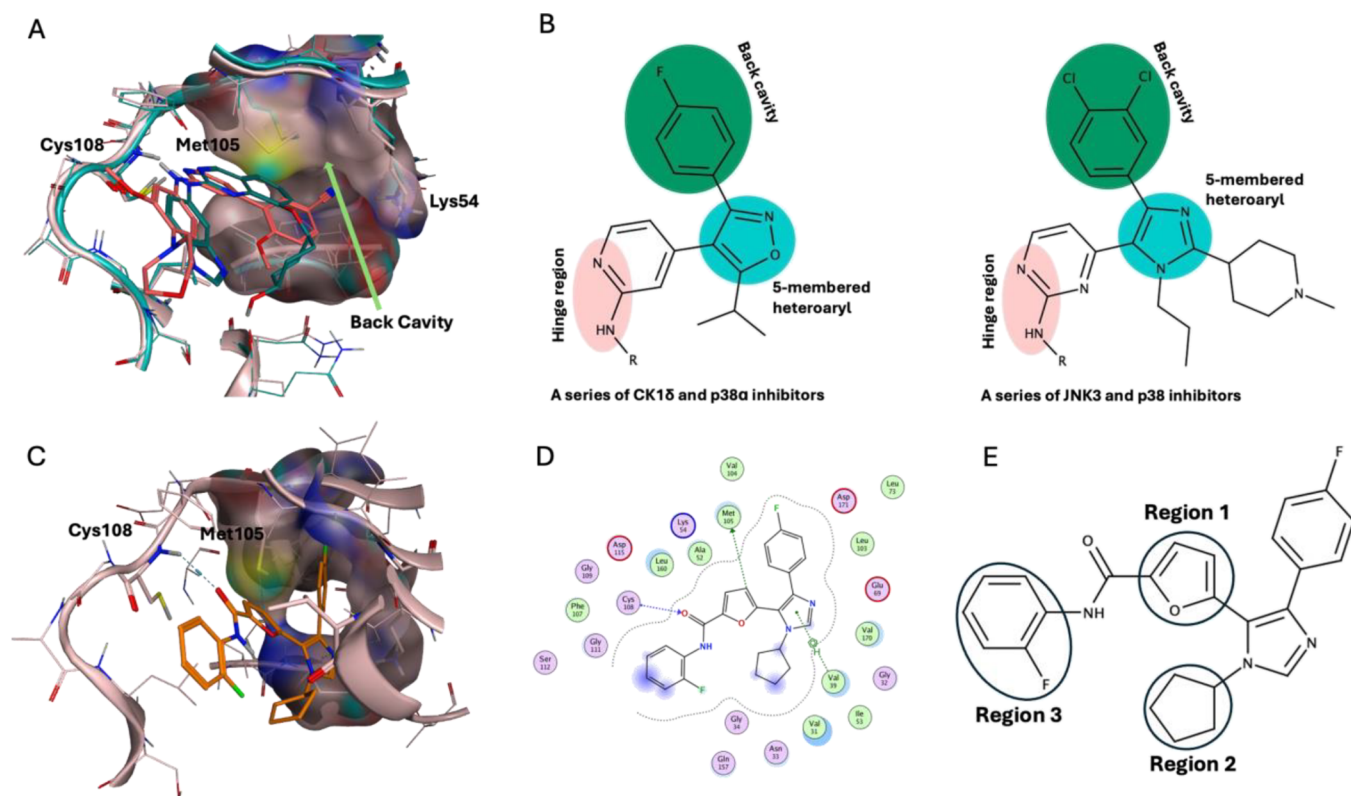


Figure 2. (A) Superposition of two TNK cocrystal structures 5D7A (protein and compound 1 in cyan) and 5AX9 (protein and compound 2 in pale pink and coral, respectively); green arrow indicates the TNK back cavity. (B) 2D pharmacophore representations of CK1 δ and JNK3 inhibitors interacting with kinase back cavities. (C) Binding mode of compound 5 with TNK; (D) 2D diagram (generated with MOE) illustrating protein–ligand interactions between compound 5 and TNK. (E) The general idea of SAR exploration.

signaling pathway, which is crucial for tissue repair and regeneration, could be affected by TNK's role in stabilizing the T-cell factor 4 (TCF4)/ β -catenin complex, potentially influencing the abnormal tissue repair characteristic of IPF.²² The JNK pathway, involved in epithelial cell death, inflammation, and collagen production, also implicates TNK in fibrogenesis.²³ Furthermore, TNK has also been associated with Hippo signaling and TNK inhibition can induce the downregulation of yes-associated protein (YAS) and transcriptional coactivator with PDZ-binding motif (TAZ).^{24,25} It was also shown that TNK plays a critical role in the regulation of procollagen trafficking and liver fibrogenesis.²⁶

More recently, TNK has been identified as an essential regulator of glucose and lipid metabolism in both vertebrate and invertebrate model organisms. These findings suggest that targeting TNK signaling could be beneficial in treating obesity and type 2 diabetes.²⁷ Considering TNK's involvement in a multitude of biological processes associated with the hallmarks of aging,²⁸ the development of new therapeutics modulating

TNK signaling has emerged as an attractive approach for treating age-related diseases.²⁹

Herein, we report the lead optimization of 4-phenylimidazole-based TNK inhibitors and the consequent discovery of 4. Currently, compound 4 is being evaluated in two phase II trials for the treatment of IPF (NCT05975983 and NCT05938920).

RESULTS AND DISCUSSION

TNK Protein Structure and Design Strategy. TNK inhibitors 1 and 2 were cocrystallized with the TNK kinase domain.¹³ Both compounds bind in the ATP-binding site engaging a hydrogen bridge with the donor backbone NH of Cys108 in the hinge region, and could be utilized as templates for generative design. However, forecasting a main challenge in the development of ATP-competitive kinase inhibitors—a decent selectivity profile, we were seeking approaches to modulate it from the beginning. It has been demonstrated that targeting a back pocket adjacent to the active site can be an effective strategy for modulating selectivity.³⁰ TNK is characterized by the gatekeeper residue Met105 which controls

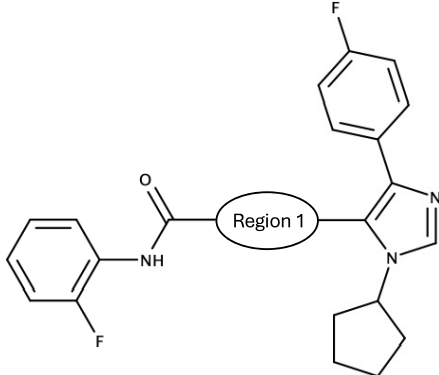
the access to the back cavity lined by the side chains of Met105, Leu103, Leu73, Tyr85, and Lys54. In the cocrystal structures 5AX9 and 5D7A, the Met105 side chain prevents pocket occupation (Figure 2A). The analysis of inhibitors of other kinases characterized by a methionine gatekeeper revealed ligand-induced conformational changes in a Met side chain allowing an inhibitor to occupy a back cavity. For instance, two series of CK1 δ and JNK3 inhibitors were reported to be able to change the orientation of the Met gatekeeper side chain.^{31,32} Noteworthy, compounds of both series share similar pharmacophore patterns, in particular: (1) a halogen-substituted phenyl situated in a back pocket, and (2) a five-membered heteroaryl that provides directional vectors to place substituents (Figure 2B). Motivated by these examples, we hypothesized that a similar strategy could be exploited to access the TNIK back cavity.

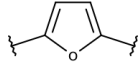
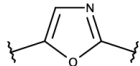
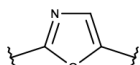
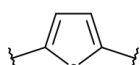
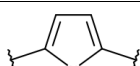
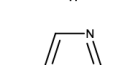
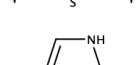
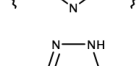
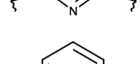
Based on the available crystal structures, we built a TNIK model with an opened back pocket and utilized it along with the structure-based drug design (SBDD) workflow of our AI-driven generative platform Chemistry42.^{33–35} Virtual structures were prioritized based on the following criteria: (1) a hydrogen bond acceptor (HBA) engaging a bond with the NH of Cys108; (2) a lipophilic aromatic function occupying the back cavity, preferably phenyl or halogen-substituted phenyl; (3) a five-membered heteroaryl linking pharmacophore points (1) and (2). Chemistry42 modeling suggested furan-2-carboxamides as a promising scaffold for TNIK inhibitors and showed a reasonable binding mode for the primary hit compound **5** (Figures 2C and 2D). Its carbonyl was predicted to form a key hydrogen bonding with the NH of Cys108, while 4-fluorophenyl was accommodated by the back pocket making a ring face $S \cdots \pi$ interaction with the Met105 sulfur. Importantly, the furan O and carboxamide NH were suggested to make an intramolecular hydrogen bond that can stabilize a planar conformation of the hinge-binding moiety. Both 2-fluorophenyl and cyclopentyl were situated in solvent-accessible parts of the catalytic site. The imidazole ring represented a well-suited linker to project functional groups. This compound was tested in the radiometric inhibition assay and demonstrated a decent TNIK inhibition with IC_{50} of 18.5 nM. We utilized **5** as a template in the follow-up rounds of structure generation and investigated the structure–activity relationship (SAR) of the chemotype. We explored three regions of the initial hit compound (Figure 2E): furan replacements (region 1), substitutions of the imidazole N1 (region 2), and carboxamide substitutions (region 3).

Preliminary SAR Exploration. The replacement of furan-2-carboxamide core (region 1 in Figure 2E) with oxazole-5- and oxazole-2-carboxamides resulted in compounds **6a** and **6b** demonstrating a significant inhibitory activity drop to a micromolar range (Table 1). It was hypothesized that **6a** showed a 100-fold lower potency than **5** because the oxazole-oxygen atom is a weaker HBA than the furan-oxygen atom due to the electron-withdrawing effect of the oxazole nitrogen. Thus, the bioactive planar conformations of the oxazole-5-carboxamide derivative are less frequently populated compared to those of furan-based structures. Compound **6b** adopts a *syn* conformation (Supporting Information) due to a stronger intramolecular hydrogen bond between the amide NH and the oxazole-nitrogen atom compared to the oxazole-oxygen atom. This preferred conformation likely contributes to its low enzymatic activity.

Compounds **6c** and **6d** were synthesized to confirm the importance of the intramolecular hydrogen bond between the

Table 1. Exploration of Core Ring Replacements (Region 1)

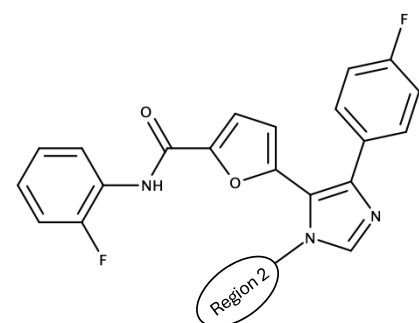


Compound	Structure	TNIK IC_{50} (nM)
5		18.5
6a		1733
6b		13835
6c		>10000
6d		>10000
6e		11693
6f		4.0
6g		>10000
6h		3.9

amide NH and an HBA of a core ring. We assumed that replacing furan with pyrrole and thiophene could lead to *syn* conformations that were supposed to be inactive. Indeed, such orientation of **6d** can be more favorable due to pyrrole NH and carbonyl contact, while the conformation of **6c** can be stabilized by the interaction between C–S σ^* orbital and the carbonyl lone pair.³⁶ Both compounds did not show activity against TNIK as expected, thus confirming a crucial role of the intramolecular hydrogen bond in the series. Thiazole-5-carboxamide **6e** and 1,2,4-triazole-3-carboxamide **6g** also displayed a weak or complete loss of activity, akin to **6c** and **6b**. Replacements with imidazole and pyridine resulted in compounds **6f** and **6h** exhibiting excellent activity against TNIK with IC_{50} values around 4 nM. These results indicate that aromatic pyridine-like nitrogen is more favorable for intramolecular hydrogen bonding with the amide NH across the tested compounds.

To explore region 2, furan derivatives with aliphatic, cycloaliphatic, and heterocycloaliphatic substituents onto the nitrogen of the imidazole linker were synthesized (Table 2).

Table 2. Exploration of Region 2



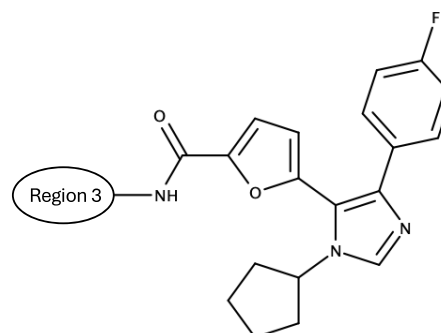
Compound	Structure	TNIK IC ₅₀ (nM)
5		18.5
7a		26.4
7b		36.9
7c		158.3
7d		63.9
7e		11.1
7f		251.3
7g		25.1
7h		76.5
7i		8452
7j		>10000

Compound 7a, obtained by inserting methylene between the cyclopentyl group and imidazole, showed a slight decrease in activity in comparison with the primary hit 5. Compounds 7b, 7g, and 7h, which contain the tetrahydrofuran moiety connected directly or through methylene to the imidazole, also exhibited slightly decreased activities. The incorporation of pyrrolidine or piperidine led to a considerable activity drop for

compounds 7c, 7f, and 7i as well as the total activity loss for 7j, indicating that the presence of a basic amine is unfavorable in this region. Compound 7d bearing cyclopropyl function demonstrated less activity than 7a. The introduction of isopropyl resulted in 7e possessing the best activity among the described analogs.

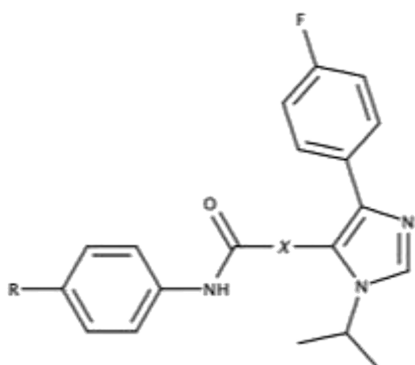
Simultaneously, we explored carboxamide substituents in the solvent-accessible region 3 (Table 3). Replacing the phenyl with pyridine generated a highly active compound 8a with an IC₅₀ of 2 nM. Compound 8b, which contains methoxy instead of fluorine at the pyridine *ortho* position, displayed even slightly improved potency. Attempts to replace the aryl function with heterocycloaliphatic groups (piperidine 8e, tetrahydropyran 8f, oxetanes 8g and 8h) led to significantly decreased activity. These

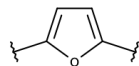
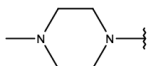

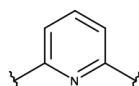
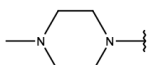
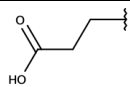
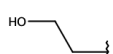
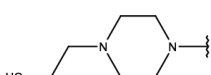
Table 3. Exploration of Region 3



Compound	Structure	TNIK IC ₅₀ (nM)
5		18.5
8a		2.0
8b		1.3
8c		>1000
8d		2.8
8e		10736
8f		1153
8g		927.7
8h		856.0

Table 4. Activity and ADME Properties of Furan and Pyridine Derivatives



Compound	X	R	TNIK IC ₅₀ (nM)	KS (μM) ^a	HLM / MLM Cl _{int(mic)} ^b
9a			10.5	40	>150 / >150
9b			40.2	<2	>150 / >150
9c			5.9	105	119.3 / 122.3
9d			5.7	<2	<9.6 / <9.6
9e			5.7	<2	160.9 / 123.5
9f			3.2	5.3	141.3 / 69.5

^aKS – kinetic solubility. ^bHLM/MLM – intrinsic clearance in human and mouse liver microsomes, μL/min/mg.

results suggest that an aromatic group in this region engages contacts that are important for tight binding. Indeed, according to the predicted binding poses of furan derivatives (Figure 2D), the 2-fluorophenyl is accommodated between Gly111 and Val31 and interacts with them through CH... π stacking. Therefore, removing a π system, as going from **8a** to **8e**, could decrease compounds' potency. Since **8a** and **8b** displayed single-digit nanomolar activity among the tested analogs, they were profiled in the kinetic solubility assay. Unfortunately, both compounds exhibited poor kinetic solubility (<2 μM). Next, we synthesized compounds **8c** and **8d** featuring polar moieties (sulfonamide and *N*-methylpiperazine respectively) at the phenyl *para* position of **5**. Interestingly, **8c** did not show obvious activity in the nanomolar range. Compound **8d** strongly inhibited TNIK with an IC₅₀ of 2.8 nM but also possessed low solubility (<2 μM) despite the piperazine basic nitrogen.

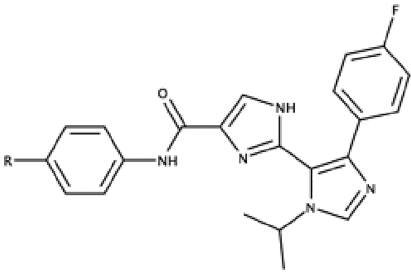
Since the incorporation of a basic amine did not improve solubility, we attempted to decrease lipophilicity. Following this strategy, we replaced cyclopentyl with isopropyl based on the SAR analysis for region 2 and removed fluorine from region 3. Compounds **9a** and **9b** exhibited good inhibitory activity with IC₅₀s of 10.5 and 40.2 nM, respectively (Table 4). Next, **9a** was submitted to the solubility assay and showed a considerable improvement (40 μM). However, there were still visible particles in the solution, indicating that further optimization is required. Moreover, profiling in human and mouse liver microsomes (HLM and MLM) revealed a high intrinsic

clearance for all furan-based derivatives ($Cl_{int(mic)} > 150 \mu\text{L}/\text{min}/\text{mg}$ for **8a**, **8b**, **8d**, **9a**, and **9b**).

Further, we conserved the structure of **9a** except for the core heteroaryl, which was replaced by pyridine and imidazole. The pyridine derivative **9c** (Table 4) demonstrated higher potency and better solubility than **9a** (105 μM with no visible particles in the solution). However, it still suffered from the high clearance in HLM and MLM. Compounds **9d** and **9e**, obtained by replacing *N*-methylpiperazine with propionic acid and 2-hydroxyethyl, displayed activity comparable to **9a** but exhibited poor solubility. Introducing *N*-(2-Hydroxyethyl)piperazine at the phenyl *para* position generated **9f**, which inhibited TNIK with IC₅₀ of 3.2 nM but possessed poor solubility and high intrinsic clearance in HLM.

Biological evaluation of bis-imidazole compound **4** revealed a promising profile (Table 5), which balanced good activity (TNIK IC₅₀ of 7.8 nM) and primary ADME properties (HLM $Cl_{int(mic)} = 25.2 \mu\text{L}/\text{min}/\text{mg}$, KS = 174 μM). Taking into account the collected SAR data, furan- and pyridine-based series were deprioritized, and the lead optimization stage was focused on the 1*H*-imidazole-4-carboxamide scaffold.

SAR Analysis of Bis-imidazole Analogs. To support the lead optimization stage, we developed a cell-based assay using LX-2, a line of immortalized primary hepatic stellate cells (HSCs). HSCs play a crucial role in maintaining extracellular matrix (ECM) and liver architecture. Upon activation, these cells transform to a myofibroblast-like phenotype and produce

Table 5. TNIK Inhibitory Activity, Potency, and Cytotoxicity in LX-2 Cells for Bis-imidazole Analogs


Compound	Structure	TNIK IC ₅₀ (nM)	LX-2 COL1 / α -SMA IC ₅₀ (μ M)	LX-2 CC ₅₀ (μ M)
4		7.8	0.063 \pm 0.038 / 0.123 \pm 0.021 (n=2) ^a	78.1
10a		148.8	>10 / >10	>100
10b		46.3	>10 / >10	>100
10c		51	>10 / >10	>100
10d		39.5	0.306 / 0.264	>100
10e		79.1	0.839 / 0.904	>100
10f		11.1	0.081 / 0.065	40.5
10g		21.1	0.123 / 0.162	>100
10h		199.1	ND	ND
10i		10.6	ND	ND
10j		34.3	0.115 / >10	>100
10k		18.0	0.071 / 0.071	12.3
10l		47.0	0.898 / 0.713	>100
10m		6.0	0.144 / 0.572	>100
10n		42.0	0.519 / 0.125	>100
10o		4.0	0.042 / 0.077	22.6

^aThe data represent averages of *n* independent experiments and are reported as mean and standard deviation.

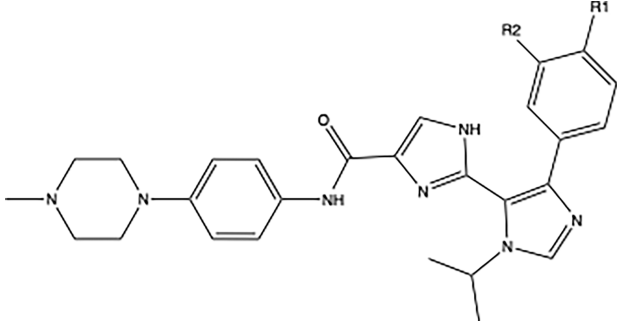
ECM proteins that lead to a fibrotic process in the liver. In this secondary assay, treatment with TGF- β was utilized to activate a

fibrogenic phenotype of LX-2 cells. The expression of α -smooth muscle actin (α -SMA) and collagen type 1 (COL1), as well as cytotoxicity, were monitored as readouts after compound treatment.

Results of profiling bis-imidazole-based derivatives are collected in Table 5. Compound 4 inhibited COL1 and α -SMA expression in LX-2 cells with IC₅₀s of 63 and 123 nM, respectively. Additionally, 4 exhibited low cytotoxicity in the same cell line (CC₅₀ of 78.08 μ M) with a safety window (CC₅₀/IC₅₀) of more than 635. Compounds 10a, 10b, and 10c bearing benzoic, 3-phenylpropanoic, and 5-phenylpentanoic acids respectively, showed decreased but still decent activity in the enzymatic assay but no efficacy in LX-2. The introduction of a negatively charged group could dramatically affect the membrane permeability of these compounds and thus explain the discrepancy between enzymatic and cell-based assays. *In vitro* evaluation of 10a, 10b, and 10c in the Caco-2 assay confirmed this hypothesis. All three compounds displayed low *P*_{app} values within 0.07–0.20 \cdot 10^{−6} cm/s. Replacement of acidic moieties with 2-hydroxyethyl and bis(2-hydroxyethyl)amino groups (10d and 10e) restored potency in LX-2 but it was lower than that for 4.

Next, we examined the effect of various piperazine substituents. Compound 10f, obtained from 4 by removing methyl, showed good activity in both TNIK and LX-2 assays, however, it also displayed higher cytotoxicity. Compared to 4, adding 2-hydroxyethyl (10g) reduced cellular potency. The inhibitory activity of 10h dropped 11-fold, and therefore this compound was not profiled in LX-2. Sulfonamide-based compound 10i demonstrated high activity but very poor kinetic solubility (<2 μ M). Intriguingly, 10j containing oxidized *N*-methylpiperazine decently inhibited TNIK kinase activity and COL1 expression in LX-2 but did not affect α -SMA production. Piperazine modifications of 10k and 10o resulted in better or comparable enzymatic and cellular potency compared to 4. On the other hand, both compounds showed higher cytotoxicity, 6- and 3.5-fold, respectively. Compounds 10l, 10m, and 10n showed a loss in the inhibition of either COL1 or α -SMA protein expression.

Finally, we synthesized compounds 11a, 11b, and 11c to investigate the impact of substituents on the phenyl ring occupying the TNIK back cavity (Table 6). Since the back pocket is mostly lined by lipophilic side chains, only hydrophobic groups were utilized. Incorporating additional fluorine at

Table 6. Exploration of R1 and R2 Phenyl Substitutions


Compound	R1	R2	TNIK IC ₅₀ (nM)
11a	F	F	51
11b	CF ₃	H	>10000
11c	Cl	H	71.3

the *meta* position (11a) led to an almost 3-fold reduction in enzymatic activity compared to 4. Interestingly, replacing fluorine with trifluoromethyl (11b) resulted in a complete loss of activity, whereas the introduction of chlorine (11c) in the same position dropped activity 4-fold. These results can be explained by a limited volume of the back pocket. Given the overall SAR analysis and the results of preliminary *in vitro* ADME screening, compound 4 was selected for further studies.

In Vitro and In Vivo ADME Profiling. Table 7 summarizes the *in vitro* ADME properties of 4. The compound exhibited

Table 7. Physicochemical Properties and *In Vitro* ADME Profile of Compound 4

Assay	Result
KS@pH 7.4 (μM)	174.0 ± 5.7 ($n = 2$) ^a
logD@pH 7.4	2.82
HMS $\text{Cl}_{\text{int(liver)}}$ h/m/r/d (mL/min/kg)	24.2/96.2/101/71
PPB Fu h/m/r/d (%)	3.4/14.6/12.8/6.2
CYP1A2, 2C9, 2C19, 2D6, 3A4-M inhibition IC_{50} (μM)	>50, > 50, 29.7, > 50, 31.6
PXR activation fold at 0.1, 1, 10 μM	0.9, 0.9, 0.7
hERG inhibition at 10 μM (%)	10.56 ± 6.47 ($n = 2$) ^a
Ames	Negative
<i>In vitro</i> safety panel, IC_{50} or EC_{50} (μM)	>10 across 78 targets except for LCK (0.31), VEGFR2 (3.5), and CHRM1 (8.4)

^aThe data represent averages of n independent experiments and are reported as mean and standard deviation. h/m/r/d stands for human/mouse/rat/dog.

excellent physicochemical parameters with KS of 174 μM and logD of 2.82, measured at a pH of 7.4. In the plasma protein binding assay, 4 displayed an adequate fraction unbound with sufficient recovery across four species. Metabolic stability was evaluated in human, mouse, rat, and dog hepatocytes (HMS). Compound 4 demonstrated moderate clearance relative to hepatic blood flow across four species with the longest half-life (88.3 min) in human hepatocytes and the shortest (32.8 min) in rat hepatocytes. To assess the drug–drug interaction (DDI) potential, 4 was screened against five major CYP450 isoforms as well as in the PXR-related CYP induction assay. The compound did not show considerable activity in all tests, indicating low potential for DDI.

The *in vitro* toxicity profile of 4 was also evaluated. In the hERG inhibition assay, no inhibitory activity was observed. Compound 4 did not cause mutagenic effects in the Ames study with or without metabolic activation. Furthermore, 4 was profiled in an off-target panel of 78 proteins, including GPCRs, nuclear receptors, ion channels, transporters, and various enzymes. No activity was found across these targets except for low to moderate potency against two kinases, LCK and VEGFR2, and 7-transmembrane receptor CHRM1.

In vivo pharmacokinetic (PK) studies were carried out in mouse and dog (Table 8). After intravenous dosing, plasma half-lives were 1.22 and 1.65 h in mouse and dog, respectively. Clearance in mouse (123.5 mL/min/kg) was higher compared to the assumed total clearance from the HMS study (46.5 mL/min/kg), whereas in dog (32.2 mL/min/kg) it was comparable (21.5 mL/min/kg). This indicates that clearance in mice might be less associated with hepatic clearance than in dogs. Across both species, 4 showed reasonable oral bioavailability of 44% in mouse and 22% in dog.

Table 8. Pharmacokinetic Parameters for Compound 4

Parameter	Mouse ^a	Dog ^a
Dose (mg/kg) po/iv	30/3	10/1
C_{max} (ng/mL) po	1010	536
$\text{AUC}_{0\text{--last}}$ (ng·h/mL) po/iv	1770/403	1120/512
T_{max} (h) po	0.25	0.708
$T_{1/2}$ (h) iv	1.22	1.65
Cl (mL/min/kg) iv	123.5	32.2
V_{ss} (mL/kg) iv	4650	2031.3
F%	44	22

^aFormulation: 20%w/v HP- β -CD in water.

Kinase Selectivity Profile. We have recently described the selectivity profile of 4.¹⁹ Briefly, the compound was screened at the dose of 10 μM against a panel of 430 enzymes, which consists of both protein and lipid kinases. The results of this screening were expressed as remaining kinase activity after compound treatment normalized to the DMSO control. In total, 43 human kinases with remaining activity under 20% after incubation with 4 were observed. Next, compound 4 was assayed against each of these kinases in a dose–response manner at the ATP concentration equaled to a kinase's K_{m} value. TNIK was inhibited by 4 with the highest potency (IC_{50} of 31 nM). Interestingly, the dose-dependent study did not confirm the results of single-dose screening for Aurora-B and ErbB4. Indeed, compound 4 demonstrated $\text{IC}_{50} > 10 \mu\text{M}$ against these enzymes. In addition to TNIK, five kinases were inhibited with $\text{IC}_{50} < 100$ nM, three of which were mutants (PDGFR α , Kit, and EGFR), and two were wild type (YES and ALK4). Notably, nonmutant Kit and PDGFR α were out of the 43 hit kinases list, whereas EGFR was inhibited in a micromolar range.

A series of 3,4-dihydrobenzo[*f*][1,4]oxazepin-5(2*H*)-one derivatives have been recently reported as highly potent TNIK inhibitors.¹⁴ The authors followed a compound design strategy similar to ours, but they targeted an allosteric hydrophobic cavity on the solvent-exposed side of the ATP binding pocket. This site is lined by Ile306, Ala110, Asp115, Asn119, Leu116, and His305. Lead compound 3 was obtained by the cyclization of the 2-methoxybenzamide of the primary hit compound and lengthening phenyl moiety to occupy the allosteric site. Compound 3 exhibited nanomolar activity against TNIK with an IC_{50} of 26 nM, and according to the described binding mode, its 4-fluorophenyl occupied the hydrophobic pocket. Compound 3 demonstrated good selectivity across 413 human kinases, however only kinases with remaining activity less than 4% were used for dose–response studies. Additionally, the authors profiled compound 1 in a panel of 102 kinases at the dose of 10 μM . Apparent potency (remaining kinase activity less than 20%) against more than 70 kinases was identified for 2. Given these results, 4 exhibits more favorable selectivity, confirming that targeting allosteric sites around an ATP-binding pocket is an instrumental strategy for designing highly selective kinase inhibitors.

Activity and Efficacy Studies. We employed the FRET assay to screen 4 at two higher ATP concentrations (64 μM and 2 mM) against TNIK. The elevated ATP doses led to increased IC_{50} values of 14.7 and 257.2 nM, respectively, revealing that 4 is an ATP-competitive inhibitor. Profiling in the SPR assay¹⁹ showed the excellent affinity of compound 4 to the TNIK kinase domain (K_{d} of 4.3 nM), which is consistent with the data from the primary radiometric assay (IC_{50} of 7.8 nM). Interestingly, the metabolite identification study in human hepatocytes

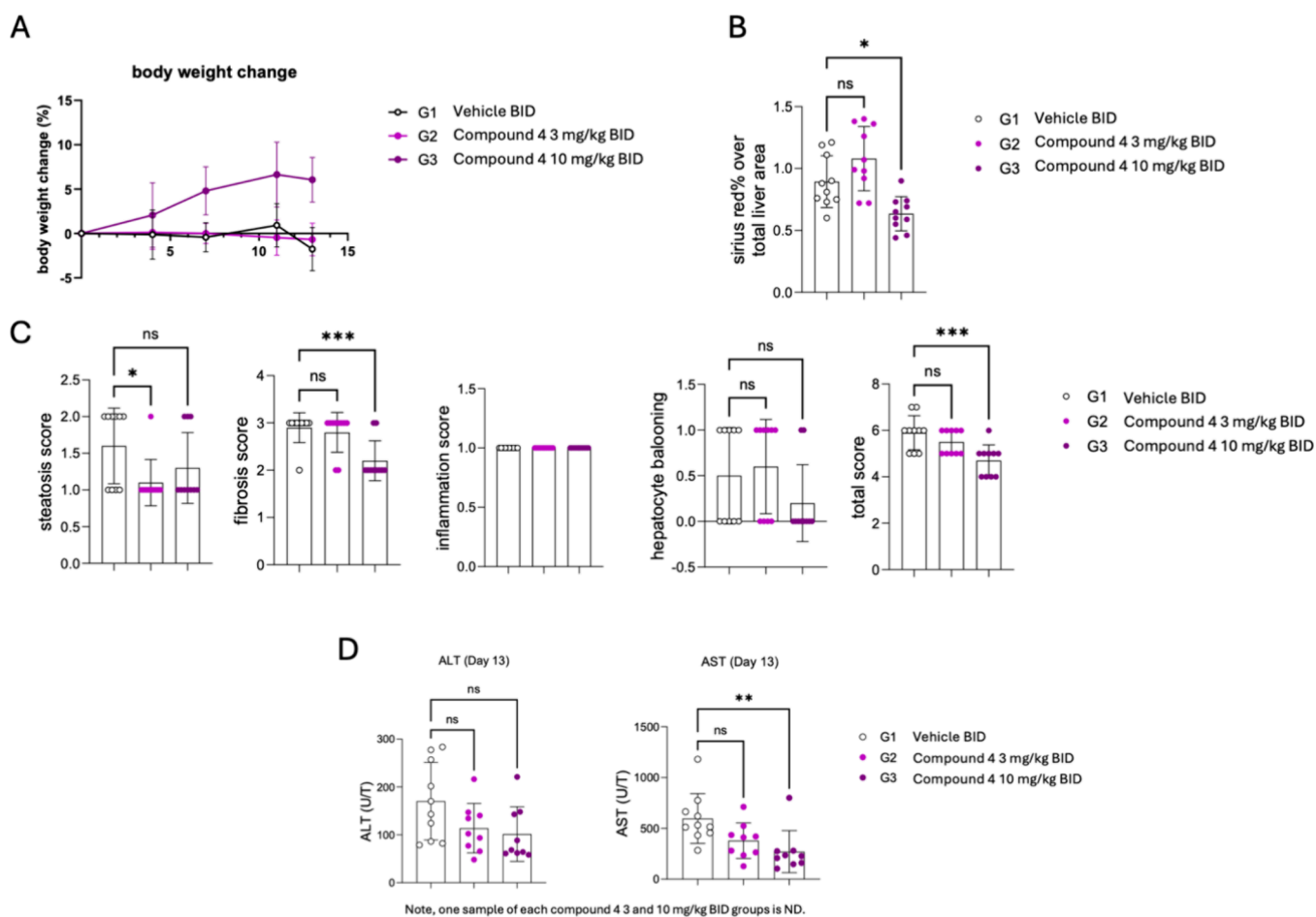


Figure 3. (A) Body weight during the study process in CCl₄-induced liver fibrosis model in C57BL/6 mice. ($n = 10$), mean \pm SD (B) Quantification of Sirius red staining of liver tissue in CCl₄-induced liver fibrosis model in C57BL/6 mice. Group 1 compared to groups 2 and 3 with $P = 0.1002$ and 0.0184 , respectively. Ordinary one-way ANOVA and post hoc Dunnett's multiple-comparison tests were used to assess statistical significance. (ns: nonspecific, *: p value < 0.05) ($n = 10$), mean \pm SD (C) Quantification of H&E staining and Sirius red staining of liver tissue in CCl₄-induced liver fibrosis model in C57BL/6 mice. 1) Steatosis score: group 1 compared to groups 2 and 3 with $P = 0.0347$ and 0.2466 , respectively; 2) fibrosis score: group 1 compared to groups 2 and 3 with $P = 0.7913$ and 0.0008 respectively; 3) inflammation score; 4) hepatocyte ballooning score: group 1 compared to groups 2 and 3 with $P = 0.8612$ and 0.3051 respectively; 4) total NAFLD score: group 1 compared to groups 2 and 3 with $P = 0.3036$ and 0.0006 , respectively; Ordinary one-way ANOVA and post hoc Dunnett's multiple-comparison test was used to assess statistical significance. (ns: nonspecific, *: p value < 0.05 ; **: p value < 0.01). ($n = 10$), mean \pm SD (D) Plasma ALT and AST levels in CCl₄-induced liver fibrosis model in C57BL/6 mice. ALT: Group 1 compared to groups 2 and 3 with $P = 0.1261$ and 0.0554 , respectively; AST: Group 1 compared to groups 2 and 3 with $P = 0.0632$ and 0.005 respectively; Ordinary one-way ANOVA and post hoc Dunnett's multiple-comparison test was used to assess statistical significance. (ns: nonspecific, **: p value < 0.01) ($n = 9$ – 10), mean \pm SD. ND: not detected for unknown reason.

(unpublished data) unveiled that compounds **10f** and **10j** are two major metabolites of **4**. Both compounds displayed decent enzymatic and cell-based activities (Table 5), which is putatively favorable for compound **4** *in vivo* efficacy profile.

The cell-based model of liver fibrosis was a handy secondary assay at the lead optimization stage. As mentioned above (Table 5), **4** exhibited good cellular potency in LX-2 cells stimulated with TGF- β , indicating the antifibrotic compound's potential. These results align with findings that TNIK promotes HSC activation, leading to fibrogenesis in the liver.²⁶ Next, compound **4** was evaluated in the cellular and animal models of lung fibrosis. The results of these studies have been comprehensively described in our recent publication.¹⁹ In short, **4** considerably reduced TGF- β -mediated α -SMA expression in lung fibroblast cells (MRC-5) with an IC₅₀ of 27 nM and the fibroblasts of donors with IPF (IC₅₀s of 50–63 nM) without substantial cytotoxicity. Additionally, compound **4** inhibited fibronectin-1 (FN-1) protein expression in human primary bronchial

epithelial cells from patients with IPF (IC₅₀s of 250–400 nM). Thus, compound **4** has been proven to mitigate TGF- β -induced epithelial-to-mesenchymal transition (EMT) and fibroblast-to-myofibroblast transition (FMT). Furthermore, **4** ameliorated fibrotic processes (more than 50% reduction in fibrotic area) and improved overall lung function (significantly reduced the respiratory parameter “enhanced pause”) in a murine bleomycin-induced lung fibrosis model. The compound's anti-inflammatory effect was confirmed in the lipopolysaccharide (LPS)-induced acute lung injury model. It considerably decreased the release of IL-1 β , IL-6, IL-7, and TNF- α . Finally, compound **4** showed an antifibrotic effect in kidney and skin fibrosis disease models.

In Vivo CCl₄-Induced Liver Fibrosis Model in Mice. The *in vivo* efficacy of compound **4** against liver fibrosis was investigated following the *in vitro* experiments with LX-2 in which **4** showed its antifibrotic potential. Carbon tetrachloride (CCl₄) is a known hepatotoxic agent used to study liver

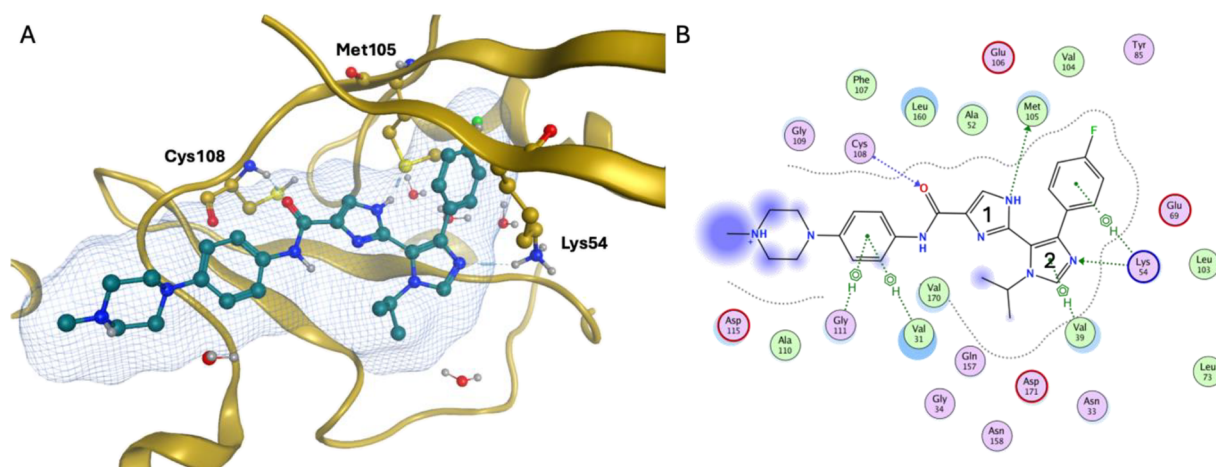
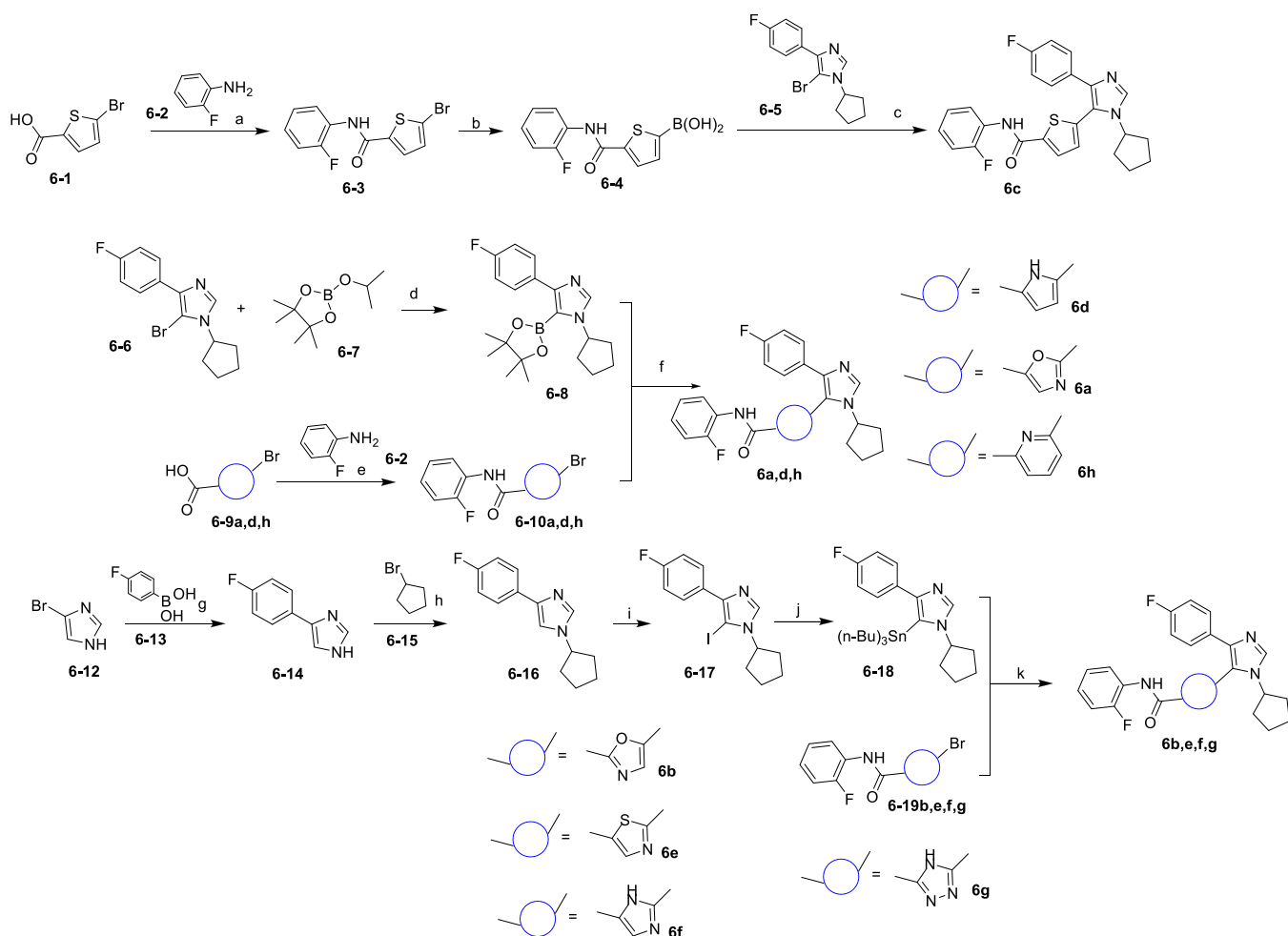


Figure 4. (A) X-ray crystal structure of compound **4** bound to the TNIK kinase domain (PDB ID: 8ZML). (B) 2D diagram (generated with MOE) illustrating protein–ligand interactions between compound **4** and TNIK.

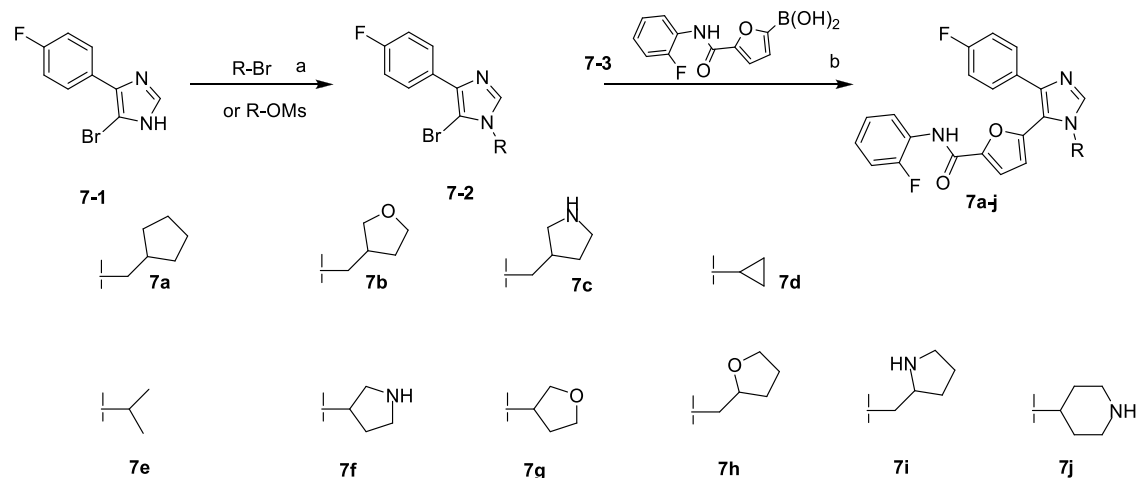
Scheme 1. Synthesis of Compounds 6a–6h^a



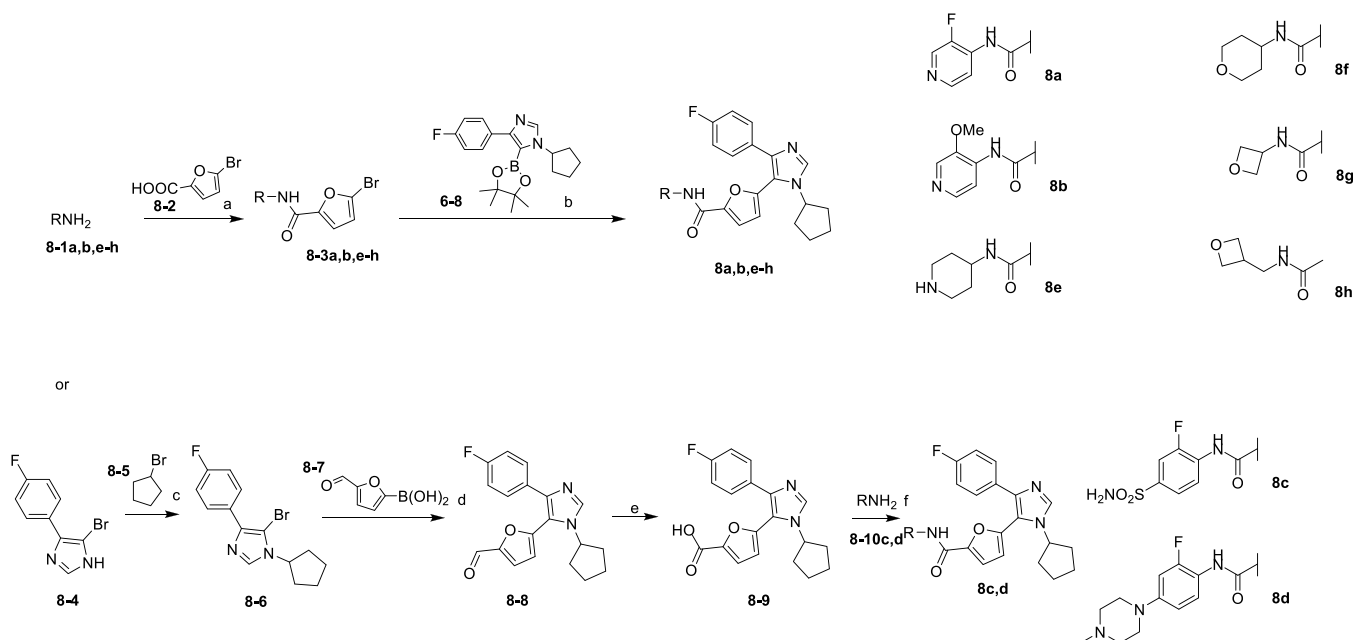
^a(a) HATU, DIEA, DMF; (b) *n*-BuLi, *i*-PrMgCl, B(OCH₃)₃, THF; 2 step; (c) APhos Pd G3, Cs₂CO₃, *t*-AmOH/H₂O; (d) *n*-BuLi, THF; (e) (COCl)₂, DMF, DCM *n*-BuLi, THF; (f) Pd(dppf)Cl₂, K₂CO₃, dioxane/H₂O; (g) Pd(PPh₃)₄, Na₂CO₃, CsF, dioxane/H₂O; (h) NaH, DMF; (i) NIS, TFA/DCM; (j) (*n*-Bu)₃SnCl, *n*-BuLi, THF; (k) Pd(PPh₃)₄, toluene.

inflammation and fibrosis.³⁷ To assess the antifibrotic effects of **4** in the liver, a mouse model of CCl₄-induced liver fibrosis was employed. After 2 weeks of treatment, average body weight changes of the vehicle group, compound **4** at 3 mg/kg BID, and

10 mg/kg BID groups were -1.8% , -0.671% , and $+6.065\%$, respectively (Figure 3A). Liver Sirius red staining for fibrosis detection showed that the group dosed with compound 4 at 10

Scheme 2. Synthesis of Compounds 7a–7j^a

^a(a) Cs₂CO₃, DMF; (b) Pd(PPh₃)₄, Na₂CO₃, CsF, dioxane/H₂O.

Scheme 3. Synthesis of Compounds 8a–8h^a

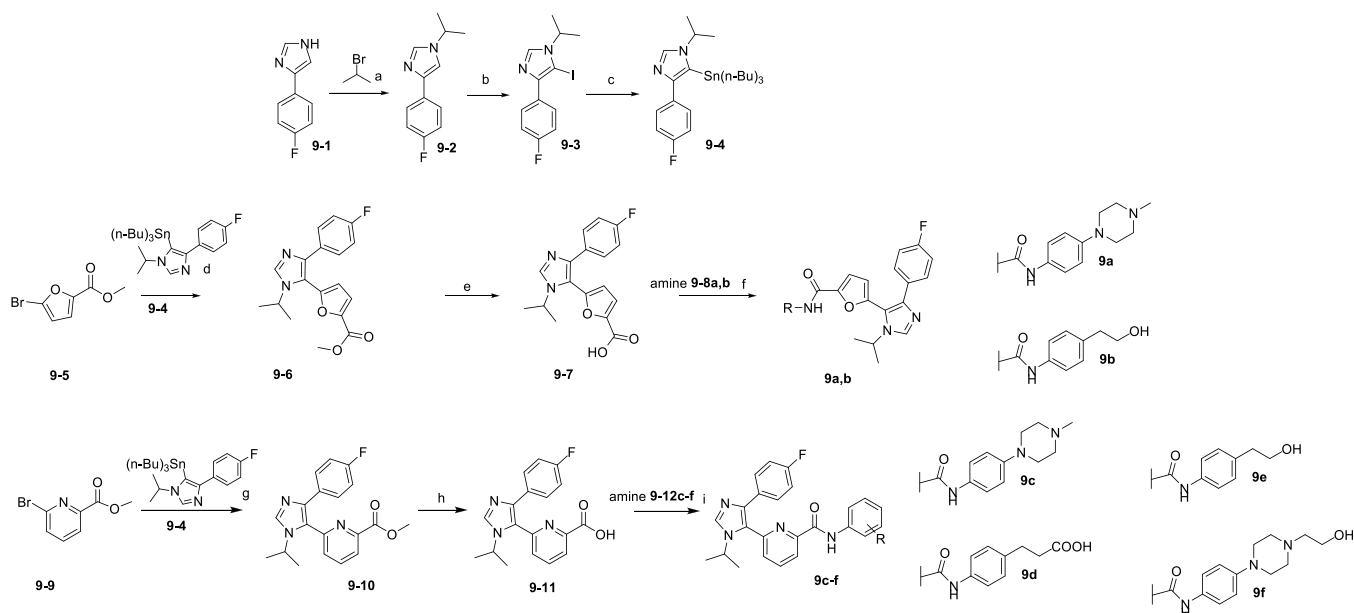
^a(a) EDCI, pyridine or HATU, DIEA, DMF; (b) Pd(dppf)Cl₂, K₂CO₃, dioxane/H₂O; (c) Cs₂CO₃, DMF; (d) XPhos-Pd-G3, K₃PO₄, DMA; (e) NaClO₂, NaH₂PO₄, *t*-BuOH, 2-methylbut-2-ene, H₂O; (f) HATU, DIPEA, DMF.

mg/kg BID exhibited a significantly lower Sirius red-stained area percentage (Figure 3B).

The liver samples were further analyzed using H&E staining. A combined analysis of H&E and Sirius red was performed for NAFLD activity scoring. As shown in Figure 3C, compound 4 at both 3 and 10 mg/kg BID reduced steatosis score and the change at 3 mg/kg BID was significant. The Inflammation scores were relatively low (=1, which means <2 foci at 20X field) in the model group and remained unchanged during the treatment. Fibrosis score was significantly reduced in the group treated with 10 mg/kg BID of compound 4, and a decreasing trend in hepatocyte ballooning score was also observed, although it was not statistically significant. Two weeks of treatment with 4 at 10 mg/kg BID resulted in a significantly lower NAFLD activity score, which is the sum of scores for steatosis, inflammation, fibrosis, and hepatocyte ballooning. Plasma ALT and AST levels

showed a decreasing trend in both the 3 and 10 mg/kg BID treatment groups (Figure 3D), with the decrease in AST in the 10 mg/kg BID group being statistically significant. Overall, compound 4 at 10 mg/kg BID ameliorated CCl₄-induced liver fibrosis and impairment.

Binding Mode of Compound 4. We solved a cocrystal structure of 4 bound to the TNIK kinase domain to validate the compound's predicted binding mode described recently.¹⁹ The X-ray study demonstrated that 4 binds to the ATP-binding site of TNIK with DFG-in and α C-helix in conformation (Figure 4). In consistency with the prediction, the carbonyl of 4 interacts with the NH of hinge Cys108 through a hydrogen bond, the NH of imidazole 1 forms a hydrogen bridge with the thiomethyl of Met105, and 4-fluorophenyl is situated in the back cavity. The pyridine-like nitrogen of imidazole 1 forms an intramolecular hydrogen bond with the carboxamide NH, thereby stabilizing a

Scheme 4. Synthesis of Compounds 9a–9f^a

^a(a) NaH, DMF; (b) NIS, TFA/DCM; (c) $(n\text{-Bu})_3\text{SnCl}$, $n\text{-BuLi}$, THF; (d) cataCXium® A Pd G3, toluene; (e) LiOH, THF, H_2O ; (f) amine, HATU, DIEA, DMF; (g) cataCXium® A Pd G3, DMA; (h) LiOH, MeOH/ H_2O ; (i) amine, HATU, DIEA, DMF.

nearly planar conformation of the hinge-binding moiety. The methylpiperazine is accommodated in the solvent-exposed region, while the proximal phenyl group is sandwiched between Gly111 and Val31. Interestingly, imidazole 2 engages a hydrogen bond with the catalytic site Lys54, forming an interaction that was not observed in the model. This interaction mimics a salt bridge between the α -phosphate of ATP and the active site Lys. Moreover, imidazole 2 pushes out the side chain of Asp171 disrupting its hydrogen bond with Lys54. A similar binding mode between imidazole and catalytic lysine was also reported for p38 α ³⁸ and TGF β R1 inhibitors.³⁹ Noteworthy, in both cases imidazole played the role of a linker, which projected moieties interacting with kinase hinge and gatekeeper regions. The isopropyl moiety of 4 was positioned in the solvent-exposed site usually occupied by the ATP ribose. To summarize, compound 4 is the first reported TNIK inhibitor, which modulates gatekeeper conformation to access and tightly interact with the allosteric back pocket.

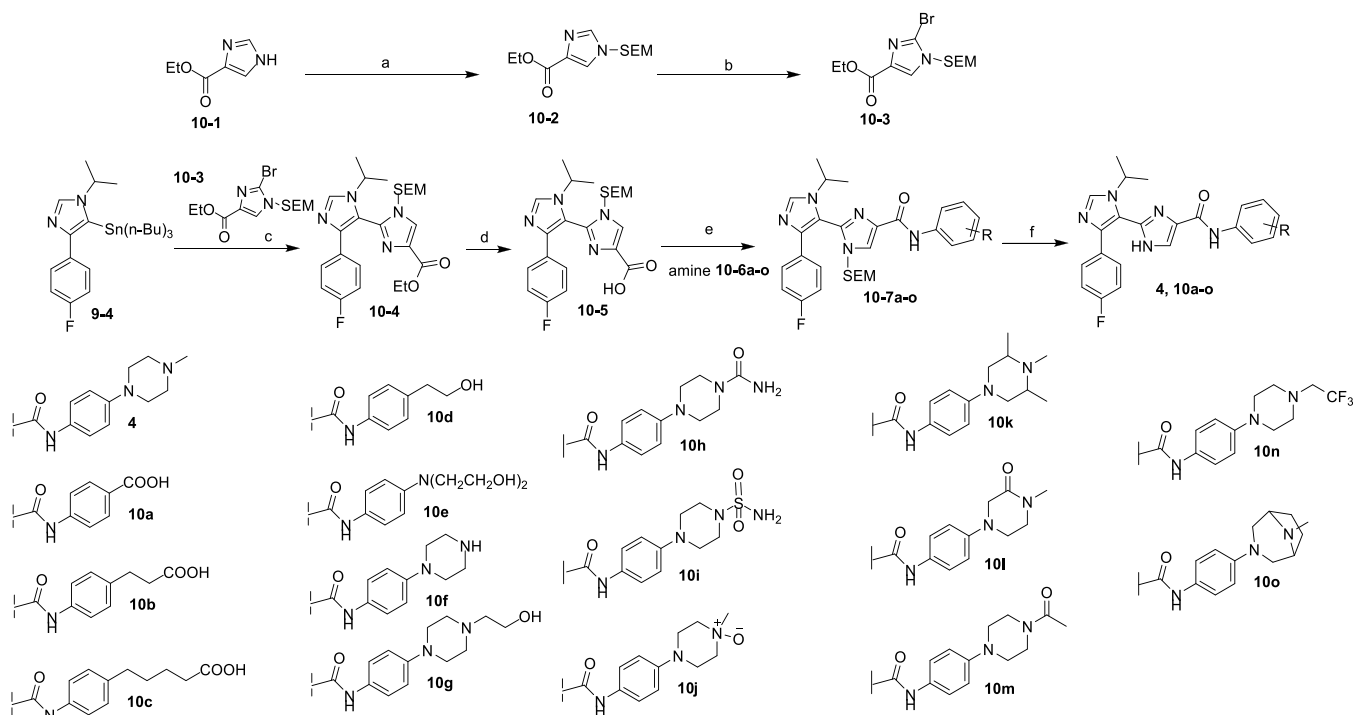
Synthetic Chemistry. The synthetic routes of compounds 6a–6h are shown in Scheme 1. Suzuki and Stille cross-coupling reactions were utilized to construct the C–C bond between the substituted imidazole ring and various N-, O-, and S-containing five- and six-membered ring heterocycles. The choice between the C–C coupling reaction types depended on the structure of the intermediates to provide the optimal yield of the final compounds and on the starting material availability. It is worth mentioning that in the case of 6f and 6g the SEM-protection group for the imidazole and triazole nitrogens was installed in the early synthesis stage and removed in the last step.

Scheme 2 presents the robust synthetic route to 7a–7j furan containing analogs with different substituents on the imidazole nitrogen. In the first stage, the substituent is implemented to the bromoimidazole nitrogen of 7-1 by a substitution reaction with the corresponding bromides (7a–7e, 7g–7i) or mesylates (7f and 7j) followed by the Suzuki coupling with the substituted furan-2-boronic acid 7-3 in the second step to result in the final compounds. Regarding compounds 7c, 7f, 7i, and 7j, the Boc-

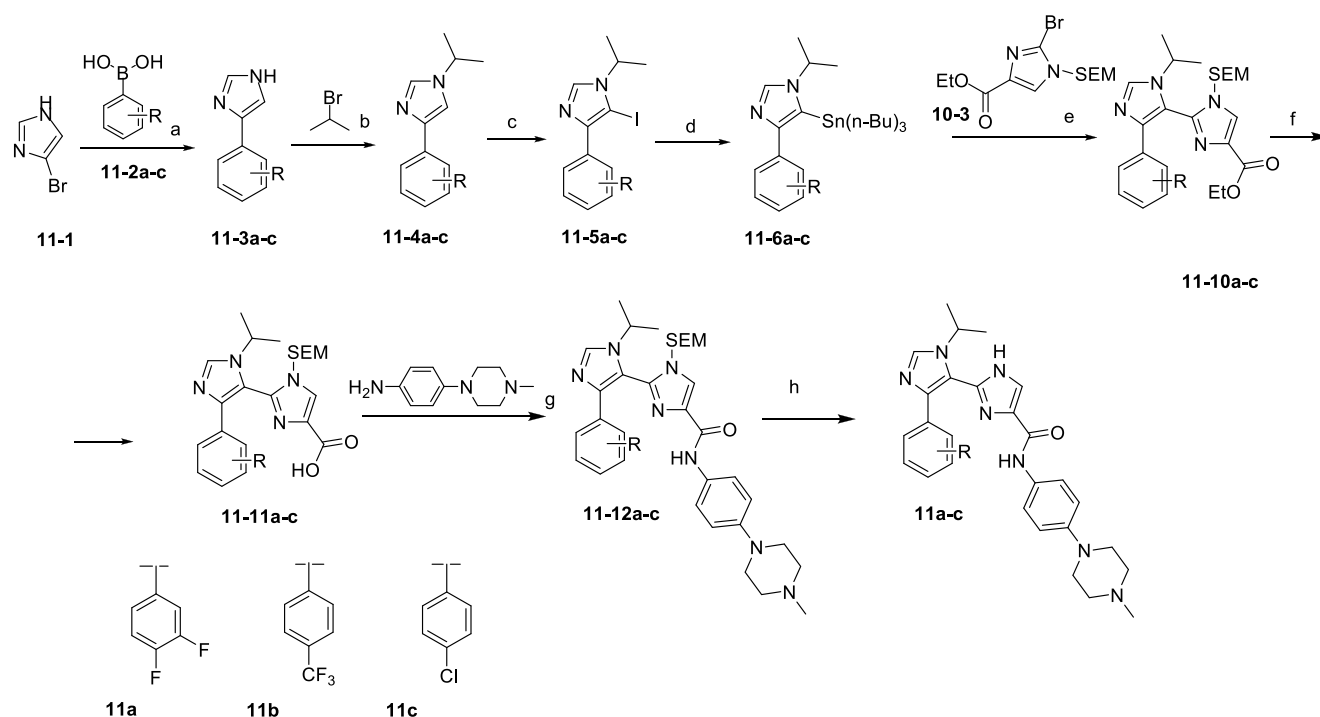
protected amino bromides or amino mesylates were used in the substitution reaction with the subsequent protection removal in the last stage. After the substitution reaction for compound 7d resulted in very low conversion, the Chan-Lam coupling was tried using the cyclopropyl boronic acid, copper(II) acetate as a catalyst, and 4,4'-bipyridine as a base in 1,2-dichloroethane to produce the corresponding substituted bromoimidazole with the acceptable conversion level (Supporting Information).

The common synthetic routes for compounds 8a–8h are represented in Scheme 3. The step sequence for the Suzuki cross-coupling depended on the starting materials in hand at the initial stage of each compound of this group. Both pathways gave reasonable yields of the final compounds. The first pathway started with an amide synthesis between corresponding amine 8-1 and 5-bromofuran-2-carboxylic acid 8-2, then obtained amide was involved in Suzuki coupling reaction with the common imidazole boronic acid pinacol ester 6-8 to produce 8a, 8b, 8e–8h. In the case of 8e, the secondary amine of aminopiperidine was *Boc*-protected and the protection was removed after the coupling. The second pathway used 5-formylfuran-2-ylboronic acid 8-7 as a “furan source” with the idea of converting the aldehyde 8-8 to the acid 8-9 and then completing the amide synthesis in the last step to generate 8c and 8d.

The synthesis of a common imidazole core intermediate 9-4 for the Stille coupling reaction is shown in Scheme 4. It required the Suzuki coupling stage between the 4-bromoimidazole and 4-fluorophenylboronic acid to form 9-1, followed by a substitution reaction to obtain *N*-substituted imidazole derivative 9-2, which was iodinated and finally converted to the Stille reagent 9-4 in the commonly known conditions. This reagent was used in Stille coupling reactions with either 5-bromofuran-2-carboxylate 9-5 for 9a and 9b or methyl 6-bromopicolinate 9-9 for 9c–9f depending on a desirable structure. Then, the ester group was hydrolyzed to the acid group and both synthetic pathways ended with the amide syntheses with corresponding amines specified in Scheme 4. For

Scheme 5. Synthesis of Compounds 4 and 10a–10o^a

^a(a) SEM-Cl, NaH, THF; (b) NBS, AIBN, CHCl₃; (c) cataCXium® A Pd G3, toluene; (d) LiOH, THF/H₂O; (e) amine, HATU, DIPEA, DMF; (f) TFA, DCM.

Scheme 6. Synthesis of Compounds 11a–11c^a

^a(a) Pd(dppf)Cl₂, K₂CO₃, CsF, dioxane/H₂O; (b) NaH, DMF; (c) NIS, TFA/DCM; (d) (n-Bu)₃SnCl, n-BuLi, THF; (e) cataCXium® A Pd G2, toluene; (f) LiOH, THF/H₂O; (g) HATU, DIEA, DMF; (h) TFA, DCM.

compound 9d, the methyl ester of the corresponding carboxylic acid was used from the first step and the methyl group was removed on the last stage.

Scheme 5 shows a common synthetic route for compounds 4 and 10a–10o. The synthesis of the second common reagent is also demonstrated in Scheme 5 – the ethyl 1H-imidazole-5-carboxylate 10-1 was SEM-protected and then brominated to

give **10–3**. After the Stille coupling reaction produced the common intermediate **10–4** and it was successfully hydrolyzed to the carboxylic acid **10–5**, the different amines were reacted with it to form the corresponding SEM-protected amides **10–7a–o**. To synthesize compounds **10a–c** containing carboxylic groups, the corresponding methyl esters were used in the amide coupling stage, then the methyl groups were removed. The deprotection reaction in the last step resulted in the corresponding amides with good yields.

The synthesis of three reagents **11–6a–c**, shown in Scheme 6, was undertaken to vary the substituents in the Stille coupling reagent. The three substituted phenylboronic acids were used in the first Suzuki coupling stage, namely 3,4-difluorophenylboronic acid **11–2a** for **11a**, 4-(trifluoromethyl)phenylboronic acid **11–2b** for **11b**, and 4-chlorophenylboronic acid **11–2c** for **11c**. After the Stille coupling between the common intermediates **11–6** and **10–3** was completed, the ester group was hydrolyzed. Then, the amide coupling was carried out followed by SEM removal to generate the final compounds **11a–c**.

CONCLUSIONS

TNIK is a promising therapeutic target against fibrosis-driven disorders such as IPF. Considering the lack of antifibrotic medications, it is desirable to develop novel selective TNK inhibitors. In this study, the compound design strategy was rationalized by analyzing available TNK kinase domain cocrystal structures, other kinases characterized by Met gatekeeper, and their known inhibitors. We utilized an AI-enabled SBDD workflow and medicinal chemistry expertise to generate an attractive starting point and optimize it to a drug candidate INS018_055. Compound **4** proved to be a highly active TNK inhibitor with desired DMPK properties. The X-ray study confirmed our modeling efforts and provided structural insights in the binding mode of **4**. This inhibitor binds to the TNK hinge region through the carboxamide rather than conventional heteroaryl-based moieties. Multiple protein–ligand interactions explain its excellent binding affinity, while the occupation of the back cavity resulted in the compound's high selectivity. Compound **4** was evaluated in multiple fibrosis and inflammation cell-based and animal models, demonstrating a considerable pan-antifibrotic and anti-inflammation effect.¹⁹ Two phase I trials demonstrated that **4** is well tolerated and safe in healthy volunteers as well as exhibits good oral bioavailability and dose-proportional PK. Currently, compound **4** is being evaluated in phase II trials in IPF.

EXPERIMENTAL SECTION

General Methods for Chemistry. Unless otherwise noted, solvents and reagents were obtained from commercial suppliers and were used without further purification. Structures of the target compounds in this work were assigned by the use of nuclear magnetic resonance (NMR) and MS spectroscopy. NMR spectra were recorded on a Bruker 400 (400 MHz ¹H, 400 MHz ¹⁹F) and were referenced in parts per million (ppm, δ). The chemical shifts are frequency referenced relative to the residual undeuterated solvent peaks. Coupling constants *J* are given in Hertz as positive values regardless of their real individual signs. The multiplicity of the signals is indicated as “s”, “d”, “t” or “m” for singlet, doublet, triplet or multiplet, respectively. LC/MS spectra were obtained using Agilent 1200/G1956A or SHIMADZU LCMS-2020. HPLC spectra were obtained using SHIMADZU LC-20AB. The purities of the final compounds are greater than 95% based on HPLC.

Synthesis of 6c. Step 1. 5-Bromo-N-(2-fluorophenyl)thiophene-2-carboxamide **6–3**. To a solution of 5-bromothiophene-2-carboxylic acid **6–1** (0.5 g, 2.41 mmol, 1.0 eq) and 2-fluoroaniline **6–2** (295.17

mg, 2.66 mmol, 1.1 eq) in DMF (5 mL) was added HATU (1.19 g, 3.14 mmol, 1.3 eq) and DIEA (624.23 mg, 4.83 mmol, 2 eq). The mixture was stirred at 20 °C for 16 h. The reaction mixture was quenched by H₂O (20 mL) and extracted with EA (6 mL \times 3). The combined organic layers were washed with brine (4 mL \times 3), dried over Na₂SO₄, filtered and concentrated under reduced pressure to give a residue. The residue was purified by column chromatography (SiO₂, PE/EOAc = 1:0 to 0:1). 5-Bromo-N-(2-fluorophenyl)thiophene-2-carboxamide **6–3** (1.02 g, 3.40 mmol, 70% yield) was obtained as a brown solid. LC-MS: RT = 0.934 min; *m/z* = 301.9 [M+H⁺].

Step 2. 5-(2-Fluorophenylcarbamoyl)thiophen-2-ylboronic acid **6–4**. To a solution of *i*-PrMgCl (2M, 832.93 μ L, 0.5 eq) in THF (20 mL) *n*-BuLi (2.5 M, 1.33 mL, 1.0 eq) was added at 0 °C. The mixture was stirred at 0 °C for 30 min. 5-Bromo-N-(2-fluorophenyl)thiophene-2-carboxamide **6–3** (1 g, 3.33 mmol, 1.0 eq) was added to the mixture at –20 °C and stirred for 30 min. Then B(OCH₃)₃ (1.38 g, 13.33 mmol, 1.51 mL, 4 eq) was added to the mixture at –20 °C. The resulting mixture was stirred at 20 °C for 2 h then quenched by aq. NH₄Cl (30 mL), and extracted with EA (15 mL \times 3). The combined organic layers were dried over Na₂SO₄, filtered and concentrated under reduced pressure to give a residue which purified by column chromatography (SiO₂, PE/EA = 1:0 to 0:1). 5-(2-Fluorophenylcarbamoyl)thiophen-2-ylboronic acid **6–4** (80 mg, 201.91 μ mol, 6.06% yield) was obtained as a light yellow solid. LC-MS: RT = 0.938 min, *m/z* = 266.0 [M+H⁺].

Step 3. 5-(1-Cyclopentyl-4-(4-fluorophenyl)-1H-imidazol-5-yl)-N-(2-fluorophenyl)thiophene-2-carboxamide **6c**. A mixture of 5-(2-fluorophenylcarbamoyl)thiophen-2-ylboronic acid **6–4** (60 mg, 226.36 μ mol, 1 eq), 5-bromo-1-cyclopentyl-4-(4-fluorophenyl)-1H-imidazole **6–5** (83.98 mg, 271.63 μ mol, 1.2 eq), Cs₂CO₃ (221.25 mg, 679.07 μ mol, 3 eq) and APHOS Pd G3 (14.38 mg, 22.64 μ mol, 0.1 eq) in *t*-AmOH (2 mL) and H₂O (0.5 mL) was degassed and purged with N₂ for 3 times. Then the mixture was stirred at 90 °C for 16 h under N₂ atmosphere. The reaction mixture was quenched by H₂O (5 mL), and extracted with EA (4 mL \times 3). The combined organic layers were dried over Na₂SO₄, filtered and concentrated under reduced pressure to give a residue. The residue was purified twice by prep-HPLC (neutral condition) and prep-HPLC (FA condition) to afford the title compound. 5-(1-Cyclopentyl-4-(4-fluorophenyl)-1H-imidazol-5-yl)-N-(2-fluorophenyl)thiophene-2-carboxamide **6c** (15.32 mg, 33.76 μ mol, 14.92% yield) was obtained as a yellow solid. ¹H NMR: (400 MHz, CDCl₃), δ = 8.42 (s, 1H), 8.02–7.91 (m, 1H), 7.75 (s, 1H), 7.69 (d, *J* = 3.6 Hz, 1H), 7.55–7.46 (m, 2H), 7.25–7.09 (m, 4H), 6.98 (t, *J* = 8.8 Hz, 2H), 4.46–4.33 (m, 1H), 2.22–2.08 (m, 2H), 1.99–1.85 (m, 4H), 1.72 (br s, 2H). ¹⁹F NMR: (400 MHz, CDCl₃), δ = –115.22 (s, 1F), –131.32 (s, 1F). LC-MS: [M+H⁺] calculated for C₂₅H₂₁F₂N₃OS: 450.15; found: 450.30.

Synthesis of 6d. Step 1. 5-Bromo-N-(2-fluorophenyl)-1H-pyrrole-2-carboxamide **6–10d**. To a mixture of 5-bromo-1H-pyrrole-2-carboxylic acid **6–9d** (420 mg, 2.21 mmol, 1 eq) in DCM (2 mL) were added DMF (161.58 mg, 2.21 mmol, 170.08 μ L, 1.0 eq) and (COCl)₂ (841.74 mg, 6.63 mmol, 580.51 μ L, 3.0 eq) at 10 °C. The mixture was stirred for 16 h at 10 °C. TLC (PE:EA = 3:1) showed a new main spot (*R*_f = 0.4) was observed and starting material was consumed. The mixture was concentrated under reduced pressure to give a residue, which was dissolved into DCM (2 mL) where DIPEA (857.11 mg, 6.63 mmol, 1.16 mL, 3.0 eq) and 2-fluoroaniline **6–2** (245.63 mg, 2.21 mmol, 213.59 μ L, 1.0 eq) were added at 10 °C. The mixture was stirred for 6 h at 30 °C. TLC (PE/EA = 3:1) showed a main spot was observed. The mixture was concentrated under reduced pressure to give a residue. The residue was purified by column chromatography on SiO₂ eluted with PE:EA = 4:1. 5-Bromo-N-(2-fluorophenyl)-1H-pyrrole-2-carboxamide **6–10d** (350 mg, crude) was obtained as a yellow solid. LC-MS: RT = 0.865 min, *m/z* = 283.0 [M+H⁺].

Step 2. 1-cyclopentyl-4-(4-fluorophenyl)-5-(4,4,5,5-tetramethyl-1,3,2-dioxaborolan-2-yl)-1H-imidazole **6–8**. To a mixture of 5-bromo-1-cyclopentyl-4-(4-fluorophenyl)-1H-imidazole **6–6** (200 mg, 646.88 μ mol, 1.0 eq) and isopropyl pinacol borate **6–7** (240.71 mg, 1.29 mmol, 263.94 μ L, 2.0 eq) in THF (4 mL) *n*-BuLi (2.5 M, 517.50 μ L, 2.0 eq) was added at –65 °C. The mixture was stirred for 1 h at –65 °C and then was allowed to warm to 10 °C stirred for 30 min. The

mixture was poured into a saturated NH_4Cl solution (50 mL) and extracted with EA (50 mL \times 2). The combined EA layers were washed with brine (50 mL), dried over Na_2SO_4 , and concentrated under reduced pressure to give 1-cyclopentyl-4-(4-fluorophenyl)-5-(4,4,5,5-tetramethyl-1,3,2-dioxaborolan-2-yl)-1H-imidazole **6–8** (320 mg, crude) as a yellow oil. LC-MS: RT = 0.872 min, m/z = 357.1 $[\text{M}+\text{H}^+]$.

Step 3. 5-(1-Cyclopentyl-4-(4-fluorophenyl)-1H-imidazol-5-yl)-N-(2-fluorophenyl)-1H-pyrrole-2-carboxamide 6d. A mixture of 5-bromo-N-(2-fluorophenyl)-1H-pyrrole-2-carboxamide **6–10d** (100 mg, 353.24 μmol , 1.0 eq), 1-cyclopentyl-4-(4-fluorophenyl)-5-(4,4,5,5-tetramethyl-1,3,2-dioxaborolan-2-yl)-1H-imidazole **6–8** (279.64 mg, 353.24 μmol , 1.0 eq), $\text{Pd}(\text{dppf})\text{Cl}_2$ (25.85 mg, 35.32 μmol , 0.1 eq) and K_2CO_3 (146.46 mg, 1.06 mmol, 3.0 eq) in dioxane (2 mL) and H_2O (0.2 mL) was stirred for 3 h at 80 °C under N_2 atmosphere. After that, the reaction mixture was filtered through SiO_2 with EA (50 mL) and the filtrate was concentrated under reduced pressure to give a residue. The residue was purified by prep-HPLC (TFA) to give 5-(1-cyclopentyl-4-(4-fluorophenyl)-1H-imidazol-5-yl)-N-(2-fluorophenyl)-1H-pyrrole-2-carboxamide **6d** (5.6 mg, 10.04 μmol , 2.84% yield) as a yellow solid. ^1H NMR: (400 MHz, $\text{DMSO}-d_6$), δ = 12.25 (br s, 1H), 10.03–9.73 (m, 1H), 8.99 (br s, 1H), 7.63 (dt, J = 2.0, 7.7 Hz, 1H), 7.51–7.39 (m, 2H), 7.36–7.17 (m, 6H), 6.49 (dd, J = 2.4, 3.5 Hz, 1H), 4.40 (quin, J = 7.2 Hz, 1H), 2.09–1.95 (m, 2H), 1.95–1.83 (m, 2H), 1.83–1.72 (m, 2H), 1.68–1.52 (m, 2H). ^{19}F NMR: (400 MHz, MeOD), δ = –117.66 (s, 1F), –125.88 (s, 1F). LC-MS: $[\text{M}+\text{H}^+]$ calculated for $\text{C}_{25}\text{H}_{22}\text{F}_2\text{N}_4\text{O}$: 433.47; found: 433.10. Other analogous **6a** and **6h** could be prepared through a similar method (Supporting Information).

Synthesis of 6e. Step 1. 4-(4-Fluorophenyl)-1H-imidazole 6–14. To a solution of 4-bromo-1H-imidazole **6–12** (10 g, 68.04 mmol, 1.0 eq) in dioxane (100 mL) and H_2O (10 mL) were added 4-fluorophenylboronic acid **6–13** (28.56 g, 204.12 mmol, 3.0 eq), Na_2CO_3 (14.42 g, 136.08 mmol, 2.0 eq), CsF (31.01 g, 204.12 mmol, 7.53 mL, 3.0 eq) and $\text{Pd}(\text{PPh}_3)_4$ (7.86 g, 6.80 mmol, 0.1 equiv) at 20 °C. The mixture was heated and stirred at 110 °C for 16 h. The mixture was added to water (200 mL) and extracted with EA (150 mL \times 3). The combined layers were concentrated in vacuum to get the residue. The residue was purified by flash SiO_2 chromatography (ISCO; 120 g SepaFlash Silica Flash Column, Eluent of 0–60% DCM/ MeOH) and concentrated in vacuum to get the 4-(4-fluorophenyl)-1H-imidazole **6–14** (13 g, 60.38 mmol, 88.74% yield) which was obtained as a yellow solid. LC-MS: RT = 0.955 min, m/z = 163.1 $[\text{M}+\text{H}^+]$.

Step 2. 1-Cyclopentyl-4-(4-fluorophenyl)-1H-imidazole 6–16. To a solution of 4-(4-fluorophenyl)-1H-imidazole **6–14** (8 g, 49.33 mmol, 1.0 eq) in DMF (40 mL) NaH (7.89 g, 197.33 mmol, 60% purity, 4.0 eq) was added at 0 °C and the mixture was stirred for 30 min, then bromocyclopentane **6–15** (29.41 g, 197.33 mmol, 21.16 mL, 4.0 eq) was added. The mixture was stirred at 80 °C for 16 h. The reaction mixture was poured into H_2O (300 mL) and extracted with EA (200 mL \times 3). The combined organic layers were washed with brine (100 mL \times 2), dried over Na_2SO_4 , filtered, and concentrated. The residue was purified by flash SiO_2 chromatography (ISCO; 330 g SepaFlash Silica Flash Column, Eluent of 0–40% Ethyl acetate/Petroleum ethergradient @ 100 mL/min) to give a spot (R_f = 0.4) as a yellow oil for the 1-cyclopentyl-4-(4-fluorophenyl)-1H-imidazole **6–16** (10 g, 43.43 mmol, 88.03% yield). ^1H NMR: (400 MHz, $\text{DMSO}-d_6$), δ = 7.95 (s, 2H), 7.82–7.77 (m, 2H), 7.67–7.59 (m, 1H), 7.58–7.50 (m, 1H), 4.61–4.45 (m, 1H), 2.23–2.00 (m, 2H), 1.94–1.45 (m, 6H).

Step 3. 1-Cyclopentyl-4-(4-fluorophenyl)-5-iodo-1H-imidazole 6–17. To a solution of 1-cyclopentyl-4-(4-fluorophenyl)-1H-imidazole **6–16** (10 g, 43.43 mmol, 1.0 eq) in DCM (30 mL), NIS (19.54 g, 86.85 mmol, 2.0 eq) and TFA (990.30 mg, 8.69 mmol, 643.05 μL , 0.2 eq) were added. The mixture was stirred at 25 °C for 1 h and after that concentrated under vacuum. The residue was purified by flash silica gel chromatography (ISCO; 330 g SepaFlash Silica Flash Column, Eluent of 0–55% Ethyl acetate/Petroleum ethergradient @ 100 mL/min) to give a spot (R_f = 0.5) as a yellow oil of 1-cyclopentyl-4-(4-fluorophenyl)-5-iodo-1H-imidazole **6–17** (9 g, 23.90 mmol, 55.04% yield). LC-MS: RT = 0.803 min, m/z = 357.1 $[\text{M}+\text{H}^+]$.

Step 4. 1-Cyclopentyl-4-(4-fluorophenyl)-5-(tributylstannyl)-1H-imidazole 6–18. To a solution of 1-cyclopentyl-4-(4-fluorophenyl)-5-iodo-1H-imidazole **6–17** (0.5 g, 1.40 mmol, 1.0 eq) in THF (5 mL) at –65 °C under N_2 - $n\text{-BuLi}$ (2.5 M, 617.67 μL , 1.1 equiv) was added dropwise. Then, the solution was stirred at –65 °C for 30 min under N_2 atmosphere. After that $\text{Sn}(\text{Bu})_3\text{Cl}$ (548.33 mg, 1.68 mmol, 453.17 μL , 1.2 eq) was added dropwise at –65 °C under N_2 atmosphere. The solution was stirred at –65 °C for another 30 min. The mixture was quenched with NaHCO_3 solution (30 mL) and extracted with EA (30 mL \times 3). The organic layer was concentrated under vacuum. The residue was purified by flash SiO_2 chromatography (ISCO; 40 g SepaFlash Silica Flash Column, Eluent of 0–100% Ethyl acetate/Petroleum ethergradient @ 80 mL/min) and judged by TLC (PE/EA = 1:1, R_f = 0.5). 1-Cyclopentyl-4-(4-fluorophenyl)-5-(tributylstannyl)-1H-imidazole **6–18** (0.38 g, 365.86 μmol , 26.06% yield) was obtained as white solid. LC-MS: RT = 1.134 min, m/z = 521.2 $[\text{M}+\text{H}^+]$.

Step 5. Ethyl 2-(1-Cyclopentyl-4-(4-fluorophenyl)-1H-imidazol-5-yl)thiazole-5-carboxylate. To a solution of 1-cyclopentyl-4-(4-fluorophenyl)-5-(tributylstannyl)-1H-imidazole **6–18** (260 mg, 500.65 μmol , 1.0 eq) and ethyl 2-bromothiazole-5-carboxylate (590.98 mg, 2.50 mmol, 5.0 eq) in toluene (2.6 mL) $\text{Pd}(\text{PPh}_3)_4$ (57.85 mg, 50.07 μmol , 0.1 eq) was added. The mixture was stirred at 100 °C for 16 h under N_2 atmosphere. TLC (PE/EA = 1:1) showed one spot of desired product formed. The mixture was concentrated under vacuum. The residue was purified by prep-TLC (SiO_2 , PE/EA = 1:1). 2-(1-Cyclopentyl-4-(4-fluorophenyl)-1H-imidazol-5-yl)thiazole-5-carboxylate (50 mg, 70.05 μmol , 13.99%) was obtained as yellow oil. LC-MS: RT = 0.809 min, m/z = 386.1 $[\text{M}+\text{H}^+]$.

Step 6. 2-(1-Cyclopentyl-4-(4-fluorophenyl)-1H-imidazol-5-yl)thiazole-5-carboxylic Acid. To a solution of 2-(1-cyclopentyl-4-(4-fluorophenyl)-1H-imidazol-5-yl)thiazole-5-carboxylate (50 mg, 70.05 μmol , 1.0 eq) in MeOH (0.5 mL) and H_2O (0.1 mL) $\text{LiOH}\cdot\text{H}_2\text{O}$ (5.88 mg, 140.09 μmol , 2.0 eq) was added. The mixture was stirred at 25 °C for 16 h. TLC (PE/EA = 1:1) showed the starting material was consumed and one new spot formed (R_f = 0.03). The mixture was concentrated under vacuum. 2-(1-Cyclopentyl-4-(4-fluorophenyl)-1H-imidazol-5-yl)thiazole-5-carboxylic acid (70 mg, crude) was obtained as yellow solid. LC-MS: RT = 0.662 min, m/z = 358.1 $[\text{M}+\text{H}^+]$.

Step 7. 2-(1-Cyclopentyl-4-(4-fluorophenyl)-1H-imidazol-5-yl)-N-(2-fluorophenyl)thiazole-5-carboxamide 6e. To a solution of 2-(1-cyclopentyl-4-(4-fluorophenyl)-1H-imidazol-5-yl)thiazole-5-carboxylic acid (60 mg, 167.88 μmol , 1.0 eq), 2-fluoroaniline (55.96 mg, 503.64 μmol , 48.66 μL , 3.0 eq) and DIEA (65.09 mg, 503.64 μmol , 87.72 μL , 3.0 eq) in DMF (0.2 mL) was added HATU (191.50 mg, 503.64 μmol , 3.0 eq). The solution was stirred at 25 °C for 1 h under N_2 atmosphere. The mixture was concentrated under vacuum. The residue was purified by prep-HPLC (column: Phenomenex Synergi C18 150*25*10 μm ; mobile phase: [water(0.225%FA)-ACN]; B γ : 38%–68%, 10 min). The product was purified by reversed-phase HPLC (0.1% TFA condition) again and dried by lyophilization. 2-(1-cyclopentyl-4-(4-fluorophenyl)-1H-imidazol-5-yl)-N-(2-fluorophenyl)thiazole-5-carboxamide **6e** (20.47 mg, 34.92 μmol , 20.80% yield, TFA salt) was obtained as yellow solid. ^1H NMR: (400 MHz, MeOD), δ = 8.61 (s, 1H), 8.11 (s, 1H), 7.69–7.63 (m, 1H), 7.49–7.39 (m, 2H), 7.34–7.07 (m, 5H), 5.12–5.06 (m, 1H), 2.28–2.12 (m, 2H), 2.03–1.85 (m, 4H), 1.82–1.66 (m, 2H). ^{19}F NMR: (400 MHz, MeOD), δ = –74.03, –75.91 (d, 3F), –115.28 (s, 1F), –124.73 (s, 1F). LC-MS: $[\text{M}+\text{H}^+]$ calculated for $\text{C}_{24}\text{H}_{20}\text{F}_2\text{N}_4\text{OS}$: 451.14; found: 451.10. Other analogous **6b**, **6f**, and **6g** could be prepared through a similar method (Supporting Information).

Synthesis of 7a. Step 1. 5-Bromo-1-(cyclopentylmethyl)-4-(4-fluorophenyl)-1H-imidazole 7–2. To a solution of 5-bromo-4-(4-fluorophenyl)-1H-imidazole **7–1** (250 mg, 1.04 mmol, 1.0 eq) and (bromomethyl)cyclopentane (253.65 mg, 1.56 mmol, 1.5 eq) in DMF (3 mL) Cs_2CO_3 (1.01 g, 3.11 mmol, 3.0 eq) was added and the mixture was stirred at 80 °C for 12 h. The residue was poured into water (50 mL). The aqueous phase was extracted with EA (20 mL \times 3). The combined organic phase was washed with brine (10 mL), dried with anhydrous Na_2SO_4 , filtered, and concentrated in vacuum. The residue was purified by prep-HPLC (column: Phenomenex Synergi C18

150*25*10um; mobile phase: [water(0.225%FA)-ACN]; B%: 53%–83%, 10 min). 5-Bromo-1-(cyclopentylmethyl)-4-(4-fluorophenyl)-1H-imidazole 7–2 (90 mg, crude) was obtained as white oil. LC-MS: RT = 0.850 min, m/z = 323.01 [M+H⁺].

Step 2. 5-(1-(Cyclopentylmethyl)-4-(4-fluorophenyl)-1H-imidazol-5-yl)-N-(2-fluorophenyl)furan-2-carboxamide 7a. To a solution of 5-bromo-1-(cyclopentylmethyl)-4-(4-fluorophenyl)-1H-imidazole 7–2 (90 mg, 278.46 μ mol, 1.0 eq) and 5-(2-fluorophenylcarbamoyl)-furan-2-ylboronic acid 7–3 (138.68 mg, 556.93 μ mol, 2.0 eq) in dioxane (1.5 mL) and H₂O (0.3 mL) was added Pd(PPh₃)₄ (32.18 mg, 27.85 μ mol, 0.1 eq), Na₂CO₃ (59.03 mg, 556.93 μ mol, 2.0 eq) and CsF (126.90 mg, 835.39 μ mol, 30.80 μ L, 3.0 eq). The mixture was stirred at 100 °C for 16 h under N₂ atmosphere. The mixture was diluted with water (30 mL) and extracted with EA (10 mL \times 2). The organic layer was concentrated and purified by prep-HPLC (column: Phenomenex Synergi C18 150*30 mm*4um; mobile phase: [water(0.05%HCl)-ACN]; B%: 34%–54%, 11 min) to give 5-(1-(cyclopentylmethyl)-4-(4-fluorophenyl)-1H-imidazol-5-yl)-N-(2-fluorophenyl)furan-2-carboxamide 7a (9 mg, 20.11 μ mol, 7.22% yield) as a white solid. ¹H NMR: (400 MHz, MeOD), δ = 7.93 (s, 1H), 7.85–7.75 (m, 1H), 7.55–7.47 (m, 2H), 7.39 (d, J = 3.6 Hz, 1H), 7.30–7.14 (m, 3H), 7.12–7.03 (m, 2H), 6.71 (d, J = 3.6 Hz, 1H), 4.08 (d, J = 7.7 Hz, 2H), 2.20 (spt, J = 7.6 Hz, 1H), 1.72–1.50 (m, 6H), 1.31–1.18 (m, 2H). ¹⁹F NMR: (400 MHz, MeOD), δ = –116.36 (s, 1F), –126.31 (s, 1F). LC-MS: [M+H⁺] calculated for C₂₆H₂₃F₂N₃O₂: 448.18; found: 448.3. Other analogous 7b–j could be prepared through a similar method (Supporting Information).

Synthesis of 8a. Step 1. 5-Bromo-N-(3-fluoropyridin-4-yl)furan-2-carboxamide 8–3a. To a mixture of 3-fluoropyridin-4-amine 8–1a (0.5 g, 4.46 mmol, 1.0 eq) and 5-bromofuran-2-carboxylic acid 8–2 (1.02 g, 5.35 mmol, 1.2 equiv) in Py (10 mL) EDCI (1.28 g, 6.69 mmol, 1.5 eq) was added at 25 °C. The mixture was stirred at 25 °C for 16 h. TLC (PE/EA = 1:1, R_f = 0.3) indicated 3-fluoropyridin-4-amine did not remain, and one major new spot with lower polarity was detected. The reaction mixture was diluted with H₂O (80 mL) and extracted with EA (15 mL \times 3). The combined organic layers were concentrated under reduced pressure to give a residue. The residue was purified by column chromatography (SiO₂, PE/EA = 5:1 to 1:1). 5-Bromo-N-(3-fluoropyridin-4-yl)furan-2-carboxamide 8–3a (1.25 g, 4.34 mmol, 97.38% yield) was obtained as a white solid. LC-MS: RT = 0.846 min, m/z = 285.1 [M+H⁺].

Step 2. 5-(1-(Cyclopentyl-4-(4-fluorophenyl)-1H-imidazol-5-yl)-N-(3-fluoropyridin-4-yl)furan-2-carboxamide 8a. To a mixture of 5-bromo-N-(3-fluoropyridin-4-yl)furan-2-carboxamide 8–3a (281.17 mg, 789.28 μ mol, 1.5 eq) and 1-cyclopentyl-4-(4-fluorophenyl)-5-(4,4,5,5-tetramethyl-1,3,2-dioxaborolan-2-yl)-1H-imidazole 6–8 (150 mg, 526.19 μ mol, 1.0 eq) in dioxane (3 mL) and H₂O (0.3 mL) was added K₂CO₃ (218.17 mg, 1.58 mmol, 3.0 eq) and Pd(dppf)Cl₂ (19.25 mg, 26.31 μ mol, 0.05 eq). The mixture was stirred at 80 °C for 2 h. The reaction mixture was quenched by saturated NH₄Cl (20 mL) at 0 °C, extracted with EA (5 mL \times 3). The combined organic layers were concentrated under reduced pressure to give a residue. The residue was purified by column chromatography (SiO₂, PE/EA = 5:1 to 0:1) to give a residue that was purified by prep-HPLC (HCl condition). 5-(1-(Cyclopentyl-4-(4-fluorophenyl)-1H-imidazol-5-yl)-N-(3-fluoropyridin-4-yl)furan-2-carboxamide 8a (12.45 mg, 28.66 μ mol, 5.45% yield) was obtained as a yellow solid. ¹H NMR: (400 MHz, MeOD), δ = 9.44 (s, 1H), 9.05–8.99 (m, 2H), 8.68 (d, J = 6.8 Hz, 1H), 7.72 (d, J = 3.6 Hz, 1H), 7.62–7.56 (m, 2H), 7.29–7.24 (m, 2H), 7.08 (d, J = 3.6 Hz, 1H), 4.88–4.84 (m, 1H), 2.35–2.26 (m, 2H), 2.13–2.05 (m, 2H), 1.99–1.91 (m, 2H), 1.84–1.76 (m, 2H). ¹⁹F NMR: (400 MHz, MeOD), δ = –111.18 (s, 1F), –135.11 (s, 1F). LC-MS: [M+H⁺] calculated for C₂₄H₂₀F₂N₄O₂: 435.16; found: 435.10. Other analogous 8b, 8e–h could be prepared through a similar method (Supporting Information).

Synthesis of 8d. Step 1. 5-Bromo-1-cyclopentyl-4-(4-fluorophenyl)-1H-imidazole 8–6. To a solution of 5-bromo-4-(4-fluorophenyl)-1H-imidazole 8–4 (1 g, 4.15 mmol, 1.0 eq) in DMF (10 mL) was added bromocyclopentane 8–5 (1.85 g, 12.45 mmol, 1.33 mL, 3.0 eq) and Cs₂CO₃ (3.38 g, 10.4 mmol, 2.5 eq). The mixture was stirred at 80 °C

for 14 h. TLC (PE/EA = 3:1) showed that the 5-bromo-4-(4-fluorophenyl)-1H-imidazole (R_f = 0.04) was consumed, and two new spots (R_f = 0.45, 0.4) were observed. The mixture was poured into water (20 mL) and extracted with EA (40 mL \times 3). The combined organic phase was washed with brine (20 mL \times 3), dried with anhydrous Na₂SO₄, filtered and concentrated in vacuum to give a residue. The residue was purified by column chromatography on SiO₂ eluted with PE/EA = 3:1. 5-Bromo-1-cyclopentyl-4-(4-fluorophenyl)-1H-imidazole 8–6 (1.05 g, 3.40 mmol, 81.9% yield) was obtained as light yellow solid. LC-MS: RT = 0.843 min, m/z = 311.1 [M+H⁺].

Step 2. 5-(1-(Cyclopentyl-4-(4-fluorophenyl)-1H-imidazol-5-yl)-furan-2-carbaldehyde 8–8. A mixture of 5-bromo-1-cyclopentyl-4-(4-fluorophenyl)-1H-imidazole 8–6 (500 mg, 1.62 mmol, 1.0 eq), (5-formyl-2-furyl)boronic acid 8–7 (340 mg, 2.43 mmol, 1.5 eq), K₃PO₄ (1.5 M, 3.24 mL, 3.0 eq) and XPhos Pd G3 (137 mg, 162 μ mol, 0.1 eq) in DMA (10 mL) was stirred for 16 h at 60 °C under N₂ atmosphere. The mixture was poured into water (40 mL) and extracted with EA (45 mL \times 2). The combined organic layers were washed with brine (15 mL \times 3), dried over Na₂SO₄, filtered and concentrated in vacuum to give a residue. The residue was purified by SiO₂ column chromatography eluted with PE/EA = 1:1 to give 5-(1-(cyclopentyl-4-(4-fluorophenyl)-1H-imidazol-5-yl)furan-2-carbaldehyde 8–8 (440 mg, 1.36 mmol, 83.7% yield) was obtained as yellow solid. LC-MS: RT = 0.784 min, m/z = 325.1 [M+H⁺].

Step 3. 5-(1-(Cyclopentyl-4-(4-fluorophenyl)-1H-imidazol-5-yl)-furan-2-carboxylic Acid 8–9. To a solution of 5-(1-(cyclopentyl-4-(4-fluorophenyl)-1H-imidazol-5-yl)furan-2-carbaldehyde 8–8 (440 mg, 1.36 mmol, 1.0 eq) in *t*-BuOH (5 mL) and H₂O (1 mL) was added NaH₂PO₄ (244 mg, 2.03 mmol, 1.5 eq), 2-methylbut-2-ene (713 mg, 10.2 mmol, 1.08 mL, 7.5 eq) and NaClO₂ (307 mg, 3.39 mmol, 2.5 eq). The mixture was stirred at 25 °C for 2 h. The mixture was diluted with water (20 mL), and adjusted with 1 N HCl solution to pH = 3. Then, some solid was precipitated, collected by filtration, and concentrated in vacuum to give crude. The crude was used in the next step without further purification. 5-(1-(Cyclopentyl-4-(4-fluorophenyl)-1H-imidazol-5-yl)furan-2-carboxylic acid 8–9 (300 mg, 881 μ mol, 65% yield) was obtained as light yellow solid. ¹H NMR: (400 MHz, DMSO-*d*₆), δ = 13.50–12.98 (m, 1H), 8.18–7.92 (m, 1H), 7.50–7.42 (m, 2H), 7.39 (d, J = 3.6 Hz, 1H), 7.21–7.10 (m, 2H), 6.91 (d, J = 3.6 Hz, 1H), 4.35 (quin, J = 7.2 Hz, 1H), 2.10–1.96 (m, 2H), 1.90–1.71 (m, 4H), 1.68–1.55 (m, 2H).

Step 4. 5-(1-(Cyclopentyl-4-(4-fluorophenyl)-1H-imidazol-5-yl)-N-(2-fluoro-4-(4-methylpiperazin-1-yl)phenyl)furan-2-carboxamide 8c. To a mixture of 5-(1-(cyclopentyl-4-(4-fluorophenyl)-1H-imidazol-5-yl)furan-2-carboxylic acid 8–9 (60 mg, 176.29 μ mol, 1.0 eq) in DMF (0.5 mL) were added DIPEA (68.4 mg, 529 μ mol, 92.1 μ L, 3.0 eq), HATU (101 mg, 264 μ mol, 1.5 eq) and 2-fluoro-4-(4-methylpiperazin-1-yl)aniline 8–10c (40.6 mg, 194 μ mol, 1.1 eq). The mixture was stirred at 25 °C for 15 h. The mixture was poured into water (15 mL). The aqueous phase was extracted with EA (20 mL \times 3). The combined organic phase was washed with brine (20 mL \times 2), dried with anhydrous Na₂SO₄, filtered, and concentrated in vacuum to give residue. The residue was purified by prep-HPLC (column: Phenomenex Luna C18 150 \times 25 mm \times 10 μ m; mobile phase: [water (0.05% HCl)-ACN]; B%: 5%–35%, 10 min) and lyophilized. 5-(1-(Cyclopentyl-4-(4-fluorophenyl)-1H-imidazol-5-yl)-N-(2-fluoro-4-(4-methylpiperazin-1-yl)phenyl)furan-2-carboxamide 8c (75.9 mg, 132 μ mol, 74.7% yield, HCl salt) was obtained as yellow solid. ¹H NMR: (400 MHz, DMSO-*d*₆), δ = 11.21 (br s, 1H), 10.22–9.92 (m, 1H), 9.90 (d, J = 1.2 Hz, 1H), 9.38 (br s, 1H), 7.74–7.52 (m, 3H), 7.45–7.29 (m, 3H), 7.10 (d, J = 3.6 Hz, 1H), 6.98 (dd, J = 2.4, 13.6 Hz, 1H), 6.84 (dd, J = 2.4, 8.8 Hz, 1H), 4.72–4.60 (m, 1H), 3.87 (br d, J = 11.2 Hz, 2H), 3.47 (br d, J = 10.8 Hz, 2H), 3.26–3.05 (m, 4H), 2.80 (d, J = 4.4 Hz, 3H), 2.20–2.04 (m, 2H), 2.03–1.90 (m, 2H), 1.89–1.74 (m, 2H), 1.73–1.52 (m, 2H). ¹⁹F NMR: (400 MHz, DMSO-*d*₆), δ = –69.20 (s, 1F), –119.60 (br s, 1F). LC-MS: [M+H⁺] calculated for C₃₀H₃₁F₂N₅O₂: 532.25; found: 532.50. The 8d analog could be prepared through a similar method (Supporting Information).

Synthesis of 9a. Step 1. 4-(4-Fluorophenyl)-1-isopropyl-1H-imidazole 9–2. To a solution of 4-(4-fluorophenyl)-1H-imidazole

9–1 (20.0 g, 123 mmol, 1.0 eq) in DMF (200 mL) was added NaH (9.87 g, 246.66 mmol, 60% purity, 2.0 eq) at 0 °C, then the mixture was stirred at 0 °C for 30 min. After that 2-bromopropane (18.20 g, 148.00 mmol, 13.90 mL, 1.2 eq) was added to the mixture at 0 °C, and the mixture was stirred at 25 °C for 17 h. The mixture was poured into water (1000 mL), extracted with EA (200 mL × 3), the organic phase was washed with brine (300 mL), dried over Na₂SO₄, filtered and concentrated to give the residue. The residue was purified by flash silica gel chromatography (ISCO; 120 g SepaFlash Silica Flash Column, Eluent of 0–50% Ethyl acetate/Petroleum ether gradient @ 100 mL/min). 4-(4-Fluorophenyl)-1-isopropyl-1H-imidazole **9–2** (21 g, 102.82 mmol, 83.37% yield) was obtained as yellow oil. ¹H NMR: (400 MHz, DMSO-*d*₆), δ = 7.81–7.75 (m, 2H), 7.74 (s, 2H), 7.33–7.07 (m, 2H), 4.42 (quin, *J* = 6.8 Hz, 1H), 1.43 (d, *J* = 6.8 Hz, 6H).

Step 2. 4-(4-Fluorophenyl)-5-iodo-1-isopropyl-1H-imidazole **9–3**. To a solution of 4-(4-fluorophenyl)-1-isopropyl-1H-imidazole **9–2** (21 g, 102.82 mmol, 1.0 eq) in DCM (210 mL) was added NIS (69.40 g, 308.46 mmol, 3.0 eq) and TFA (3.52 g, 30.85 mmol, 2.28 mL, 0.3 eq) at 10 °C, the mixture was stirred at 20 °C for 5 h. The mixture was poured into saturated Na₂SO₃ solution (500 mL), extracted with DCM (200 mL × 3), the organic phase was washed with saturated Na₂SO₃ solution (300 mL × 3) and brine (300 mL), then dried over Na₂SO₄, filtered and concentrated to give the residue. The residue was triturated in PE/EA (5:1, 100 mL) and filtered. 4-(4-Fluorophenyl)-5-iodo-1-isopropyl-1H-imidazole **9–3** (30 g, 90.87 mmol, 88.38% yield) was obtained as yellowish solid. ¹H NMR: (400 MHz, DMSO-*d*₆), δ = 8.15 (s, 1H), 7.95–7.82 (m, 2H), 7.31–7.17 (m, 2H), 4.47–4.32 (m, 1H), 1.47 (d, *J* = 6.4 Hz, 6H).

Step 3. 4-(4-Fluorophenyl)-1-isopropyl-5-(tributylstannyl)-1H-imidazole **9–4**. To a solution of 4-(4-fluorophenyl)-5-iodo-1-isopropyl-1H-imidazole **9–3** (2 g, 6.06 mmol, 1.0 eq) in THF (50 mL) was added *n*-BuLi (2.5 M, 3.15 mL, 1.3 eq) at –70 °C, the mixture was stirred at –70 °C for 30 min, then Sn(Bu)₃Cl (3.75 g, 11.52 mmol, 3.10 mL, 1.90 eq) was added to the mixture at –70 °C. The mixture was stirred at –70 °C for another 30 min. The mixture was poured into saturated KF solution (100 mL) and saturated NH₄Cl solution (100 mL), extracted with EA (50 mL × 3), the organic phase was washed with brine (50 mL) dried over Na₂SO₄, filtered, and concentrated to give the residue. The residue was purified by flash silica gel chromatography (ISCO; 120 g SepaFlash Silica Flash Column, Eluent of 0–25% Ethyl acetate/Petroleum ether gradient @ 100 mL/min). 4-(4-Fluorophenyl)-1-isopropyl-5-(tributylstannyl)-1H-imidazole **9–4** (1.2 g, 2.43 mmol, 40.14% yield) was obtained as yellow oil. ¹H NMR: (400 MHz, DMSO-*d*₆), δ = 8.07–8.00 (m, 1H), 7.41–7.32 (m, 2H), 7.23–7.15 (m, 2H), 4.16 (quin, *J* = 6.8 Hz, 1H), 1.47 (d, *J* = 6.8 Hz, 6H), 1.39–1.27 (m, 6H), 1.24–1.12 (m, 7H), 0.96–0.88 (m, 5H), 0.78 (t, *J* = 7.2 Hz, 9H).

Step 4. Methyl 5-(4-(4-Fluorophenyl)-1-isopropyl-1H-imidazol-5-yl)furan-2-carboxylate **9–6**. To a solution of methyl 4-(4-fluorophenyl)-1-isopropyl-5-(tributylstannyl)-1H-imidazole **9–4** (100 mg, 202.72 μmol, 1.0 eq) and methyl 5-bromofuran-2-carboxylate **9–5** (83.12 mg, 405.44 μmol, 2.0 eq) in toluene (2 mL) was added cataCXium A Pd G3 (20 mg, 60.91 μmol, 0.3 eq) under N₂ atmosphere at 20 °C. The mixture was stirred at 110 °C for 16 h. After that, the mixture was concentrated under reduced pressure to afford residue. The residue was purified by prep-TLC (PE/EA = 1:1) to afford desired methyl 5-(4-(4-fluorophenyl)-1-isopropyl-1H-imidazol-5-yl)furan-2-carboxylate **9–6** (65 mg, 181.54 μmol, 89.55% yield) as colorless oil. LC-MS: RT = 0.715 min, *m/z* = 329.2 [M+H⁺].

Step 5. 5-(4-(4-Fluorophenyl)-1-isopropyl-1H-imidazol-5-yl)furan-2-carboxylic acid **9–7**. To a solution of methyl 5-(4-(4-fluorophenyl)-1-isopropyl-1H-imidazol-5-yl)furan-2-carboxylate **9–6** (60 mg, 182.74 μmol, 1.0 eq) in THF (1 mL) and H₂O (0.5 mL) was added LiOH·H₂O (76.68 mg, 1.83 mmol, 10.0 eq) at 25 °C. The mixture was stirred at 25 °C for 3 h. The mixture was concentrated under reduced pressure to afford a residue. The residue was purified by prep-HPLC (column: 3 Phenomenex Luna C18 75*30 mm*3um; mobile phase: [water(0.1%TFA)-ACN]; B%: 15%–45%, 7 min) to afford crude product. 5-(4-(4-Fluorophenyl)-1-isopropyl-1H-imidazol-5-yl)furan-2-carboxylic acid **9–7** (50 mg, 155.90 μmol, 85.31% yield)

was obtained as white solid. LC-MS: RT = 0.778 min, *m/z* = 315.2 [M+H⁺].

Step 6. 5-(4-(4-Fluorophenyl)-1-isopropyl-1H-imidazol-5-yl)-N-(4-(4-methylpiperazin-1-yl)phenyl)furan-2-carboxamide **9a**. To a solution of 5-(4-(4-fluorophenyl)-1-isopropyl-1H-imidazol-5-yl)furan-2-carboxylic acid **9–7** (25 mg, 79.54 μmol, 1.0 eq) and 4-(4-methylpiperazin-1-yl)aniline **9–8a** (30.43 mg, 159.08 μmol, 2.0 eq) in DMF (1.5 mL) was added HATU (60.49 mg, 159.08 μmol, 2.0 eq) and DIEA (30.84 mg, 238.62 μmol, 41.56 uL, 3.0 eq) at 25 °C. The mixture was stirred at 25 °C for 2 h. and after that poured to H₂O (20 mL). The mixture was extracted with DCM (20 mL × 2). The combined organic layers were washed with brine (20 mL), dried over Na₂SO₄, filtered, and concentrated under reduced pressure to give a residue. The residue was purified by prep-HPLC (column: 3 Phenomenex Luna C18 75 × 30 mm × 3 μm; mobile phase: [water(0.1%TFA)-ACN]; B%: 12%–42%, 7 min) to afford desired 5-(4-(4-fluorophenyl)-1-isopropyl-1H-imidazol-5-yl)-N-(4-(4-methylpiperazin-1-yl)phenyl)furan-2-carboxamide **9a** (30.05 mg, 48.65 μmol, 61.17% yield, TFA salt) as oil. ¹H NMR: (400 MHz, DMSO-*d*₆), δ = 10.14 (s, 1H), 9.98–9.63 (m, 1H), 8.37 (br s, 1H), 7.63 (d, *J* = 8.8 Hz, 2H), 7.54–7.46 (m, 3H), 7.19 (t, *J* = 8.8 Hz, 2H), 7.04–6.97 (m, 3H), 4.27 (br d, *J* = 6.4 Hz, 1H), 3.79 (br s, 2H), 3.53 (br d, *J* = 11.4 Hz, 2H), 3.17 (br d, *J* = 8.2 Hz, 2H), 2.93 (br s, 2H), 2.87 (s, 3H), 1.45 (d, *J* = 6.8 Hz, 6H). LC-MS: [M+H⁺] calculated for C₂₈H₃₀FN₃O₂: 488.25; found: 488.3. Other analogue **9b** could be prepared through a similar method (Supporting Information).

Synthesis of 9c. Step 1. Methyl 6-(4-(4-Fluorophenyl)-1-isopropyl-1H-imidazol-5-yl)picolinate **9–10**. To a solution of 4-(4-fluorophenyl)-1-isopropyl-5-(tributylstannyl)-1H-imidazole **9–4** (500 mg, 1.01 mmol, 1.0 eq) and methyl 6-bromopyridine-2-carboxylate **9–9** (263 mg, 1.22 mmol, 1.2 eq) in DMA (8 mL) was added cataCXium A Pd G3 (73.8 mg, 101 μmol, 0.10 eq). The mixture was stirred at 95 °C under N₂ atmosphere for 12 h. The reaction mixture was diluted with water (30 mL) and extracted with EA (30 mL × 3). The combined organic layers were washed with brine (50 mL), dried over Na₂SO₄, filtered and concentrated. The residue was purified by Prep-TLC (SiO₂, PE/EA = 1:1, P: Rf = 0.35). Methyl 6-(4-(4-fluorophenyl)-1-isopropyl-1H-imidazol-5-yl)picolinate **9–10** (250 mg, 442.00 μmol, 43.61% yield) was obtained as colorless oil. LC-MS: RT = 0.759 min, *m/z* = 340.2 [M+H⁺].

Step 2. 6-(4-(4-Fluorophenyl)-1-isopropyl-1H-imidazol-5-yl)-picolinic Acid **9–11**. To a solution of methyl 6-(4-(4-fluorophenyl)-1-isopropyl-1H-imidazol-5-yl)picolinate **9–10** (250 mg, 442.00 μmol, 60% purity, 1.0 equiv) in MeOH (2.5 mL) was added LiOH (31.8 mg, 1.33 mmol, 3.0 equiv) in H₂O (0.5 mL). The mixture was stirred at 25 °C for 2 h. After that, it was adjusted to pH = 5 with 1 N HCl solution and concentrated in vacuum to give a residue. The residue was purified by prep-HPLC (column: Shim-pack C18 150 × 25 × 10 μm; mobile phase: [water (0.225%FA)-ACN]; B%: 10%–30%, 10 min). 6-(4-(4-Fluorophenyl)-1-isopropyl-1H-imidazol-5-yl)picolinic acid **9–11** (70 mg, 215.16 μmol, 48.68% yield) was obtained as white solid. LC-MS: RT = 0.748 min, *m/z* = 326.1 [M+H⁺].

Step 3. 6-(4-(4-Fluorophenyl)-1-isopropyl-1H-imidazol-5-yl)-N-(4-(4-methylpiperazin-1-yl)phenyl)picolinamide **9c**. To a solution of 6-(4-(4-fluorophenyl)-1-isopropyl-1H-imidazol-5-yl)picolinic acid **9–11** (15.0 mg, 46.1 μmol, 1.0 eq) and 4-(4-methylpiperazin-1-yl)aniline **9–12c** (17.6 mg, 92.2 μmol, 2.0 equiv) in DMF (0.1 mL) was added HATU (35.1 mg, 92.2 μmol, 2.0 eq) and DIEA (17.9 mg, 138 μmol, 24.1 uL, 3.0 equiv). The mixture was stirred at 25 °C for 1 h. The mixture was added to H₂O (8 mL) and extracted with EA (8 mL × 3). The organic phase was washed with brine (20 mL), dried over anhydrous Na₂SO₄, and concentrated in vacuum to give a residue. The residue was purified by prep-HPLC (column: 3 Phenomenex Luna C18 75 × 30 mm × 3 μm; mobile phase: [water (0.1%TFA)-ACN]; B%: 18%–38%, 7 min). 6-(4-(4-Fluorophenyl)-1-isopropyl-1H-imidazol-5-yl)-N-(4-(4-methylpiperazin-1-yl)phenyl)picolinamide **9c** (18.99 mg, 37.40 μmol, 81.13%) was obtained as yellow gum. ¹H NMR: (400 MHz, DMSO-*d*₆), δ = 10.31 (s, 1H), 9.90–9.69 (m, 1H), 8.81 (br s, 1H), 8.24–8.18 (m, 1H), 8.12 (t, *J* = 7.8 Hz, 1H), 7.75 (d, *J* = 9.0 Hz, 2H), 7.62 (dd, *J* = 0.8, 7.7 Hz, 1H), 7.45–7.36 (m, 2H), 7.20 (t, *J* = 8.8

Hz, 2H), 7.03 (d, J = 9.1 Hz, 2H), 4.67–4.56 (m, 1H), 3.83–3.80 (m, 2H), 3.53 (br d, J = 11.3 Hz, 2H), 3.17 (br d, J = 7.5 Hz, 2H), 2.94 (br t, J = 12.3 Hz, 2H), 2.87 (s, 3H), 1.48 (d, J = 6.6 Hz, 5H). LC-MS: $[M+H]^+$ calculated for $C_{29}H_{31}FN_6O$: 499.26; found: 499.30. Other analogous **9d–f** could be prepared through a similar method (Supporting Information).

Synthesis of 4. **Step 1.** Ethyl 1-((2-(trimethylsilyl)ethoxy)methyl)-1H-imidazole-4-carboxylate **10–2**. To a solution of NaH (8.56 g, 214.07 mmol, 60% purity, 1.5 eq) in THF (200 mL) was added ethyl 1H-imidazole-5-carboxylate **10–1** (20 g, 142.71 mmol, 1.0 eq) in THF (100 mL) at 0 °C. The mixture was stirred at 0 °C for 20 min, and then stirred at 20 °C for another 30 min. SEM-Cl (35.69 g, 214.07 mmol, 37.89 mL, 1.5 eq) was added to the mixture at 0 °C. The mixture was stirred at 20 °C for 16 h. The mixture was poured into saturated NH_4Cl (200 mL), and then extracted with EA (100 mL \times 2). The combined organic layer was washed with brine (20 mL \times 2), dried over Na_2SO_4 , filtered, and concentrated under reduced pressure to give a residue. The residue was purified by silica gel chromatography (PE/EA = 5:1 to 1:1). Ethyl 1-((2-(trimethylsilyl)ethoxy)methyl)-1H-imidazole-4-carboxylate **10–2** (15.9 g, 58.80 mmol, 41.20% yield) was obtained as yellow oil. 1H NMR: (400 MHz, $CDCl_3$), δ = 7.72 (d, J = 1.4 Hz, 1H), 7.61 (d, J = 1.4 Hz, 1H), 5.30 (s, 2H), 4.37 (q, J = 7.2 Hz, 2H), 3.49 (dd, J = 7.8, 8.7 Hz, 2H), 1.39 (t, J = 7.2 Hz, 3H), 0.98–0.85 (m, 2H), 0.04–0.06 (m, 10H).

Step 2. Ethyl 2-bromo-1-((2-(trimethylsilyl)ethoxy)methyl)-1H-imidazole-4-carboxylate **10–3**. To a solution of ethyl 1-((2-(trimethylsilyl)ethoxy)methyl)-1H-imidazole-4-carboxylate **10–2** (14.5 g, 53.62 mmol, 1.0 eq) in $CHCl_3$ (150 mL) was added NBS (9.54 g, 53.62 mmol, 1.0 eq) and AIBN (880.56 mg, 5.36 mmol, 0.1 eq) at 20 °C. The mixture was stirred at 60 °C for 5 h. The mixture was concentrated under reduced pressure to give a residue. The residue was purified by silica gel chromatography (PE/EA = 5:1 to 1:1). Ethyl 2-bromo-1-((2-(trimethylsilyl)ethoxy)methyl)-1H-imidazole-4-carboxylate **10–3** (11 g, 31.49 mmol, 58.73% yield) was obtained as yellow solid. 1H NMR: (400 MHz, $CDCl_3$), δ = 7.76 (s, 1H), 5.31 (s, 2H), 4.38 (q, J = 7.2 Hz, 2H), 3.61–3.49 (m, 2H), 1.38 (t, J = 7.2 Hz, 3H), 1.01–0.85 (m, 2H), 0.05–0.07 (m, 9H).

Step 3. Ethyl 5'-(4-fluorophenyl)-3'-isopropyl-1-((2-(trimethylsilyl)ethoxy)methyl)-1H,3'H-2,4'-biimidazole-4-carboxylate **10–4**. To a solution of 4-(4-fluorophenyl)-1-isopropyl-5-(tributylstannyl)-1H-imidazole **9–4** (300 mg, 608.17 μ mol, 1.0 eq) and ethyl 2-bromo-1-((2-(trimethylsilyl)ethoxy)methyl)-1H-imidazole-4-carboxylate **10–3** (318.64 mg, 912.25 μ mol, 1.5 eq) in toluene (2 mL) was added cataCXium A Pd G3 (120.00 mg, 179.47 μ mol, 2.95 eq) under N_2 atmosphere at 20 °C. The mixture was stirred at 110 °C for 16 h. Then it was concentrated under reduced pressure to afford residue. The residue was purified by prep-HPLC (column: Phenomenex luna C18 150*40 mm* 15um; mobile phase: [water(0.225%FA)-ACN]; $B\%$: 54%–64%, 14 min) to afford desired ethyl 5'-(4-fluorophenyl)-3'-isopropyl-1-((2-(trimethylsilyl)ethoxy)methyl)-1H,3'H-2,4'-biimidazole-4-carboxylate **10–4** (60 mg, 125.68 μ mol, 20.67% yield) was obtained as brown oil. LC-MS: RT = 0.920 min, m/z = 473.3 $[M+H]^+$.

Step 4. 5'-(4-Fluorophenyl)-3'-isopropyl-1-((2-(trimethylsilyl)ethoxy)methyl)-1H,3'H-2,4'-biimidazole-4-carboxylic acid **10–5**. To a solution of ethyl 5'-(4-fluorophenyl)-3'-isopropyl-1-((2-(trimethylsilyl)ethoxy)methyl)-1H,3'H-2,4'-biimidazole-4-carboxylate **10–4** (50.00 mg, 105.79 μ mol, 1.0 eq) in THF (1 mL) and H_2O (1 mL) was added $LiOH \cdot H_2O$ (8.88 mg, 211.58 μ mol, 2.0 eq) at 20 °C. The mixture was stirred at 20 °C for 4 h. 1 N HCl solution (10 mL) was added to the mixture. The mixture was extracted with EA (20 mL \times 3). The combined organic layers were washed with brine (20 mL), dried over Na_2SO_4 , filtered, and concentrated under reduced pressure to give a crude product. 5'-(4-fluorophenyl)-3'-isopropyl-1-((2-(trimethylsilyl)ethoxy)methyl)-1H,3'H-2,4'-biimidazole-4-carboxylic acid **10–5** (50 mg, crude) was obtained as colorless oil. LC-MS: RT = 0.778 min, m/z = 445.3 $[M+H]^+$.

Step 5. 5'-(4-Fluorophenyl)-3'-isopropyl-N-(4-(4-methylpiperazin-1-yl)phenyl)-1-((2-(trimethylsilyl)ethoxy)methyl)-1H,3'H-2,4'-biimidazole-4-carboxamide **10–7**. To a solution of 5'-(4-fluoro-

phenyl)-3'-isopropyl-1-((2-(trimethylsilyl)ethoxy)methyl)-1H,3'H-2,4'-biimidazole-4-carboxylic acid **10–5** (80 mg, 179.95 μ mol, 1.0 eq) and 4-(4-methylpiperazin-1-yl)aniline (51.63 mg, 269.92 μ mol, 1.5 eq) in DMF (2 mL) was added HATU (102.63 mg, 269.92 μ mol, 1.5 eq) and DIPEA (69.77 mg, 539.84 μ mol, 94.03 μ L, 3 eq) at 20 °C. The mixture was stirred at 20 °C for 1.5 h. The mixture was poured into H_2O (20 mL). The mixture was extracted with EA (20 mL \times 3). The combined organic layers were washed with brine (20 mL), dried over Na_2SO_4 , filtered and concentrated under reduced pressure to give a residue. The residue was purified by prep-HPLC (column: Phenomenex Gemini-NX C18 75*30 mm*3um; mobile phase: [water(10 mM NH_4HCO_3)-ACN]; $B\%$: 40%–70%, 8 min) to afford the desired 5'-(4-fluorophenyl)-3'-isopropyl-N-(4-(4-methylpiperazin-1-yl)phenyl)-1-((2-(trimethylsilyl)ethoxy)methyl)-1H,3'H-2,4'-biimidazole-4-carboxamide **10–7** (50 mg, 80.93 μ mol, 44.97% yield) that was obtained as colorless oil. LC-MS: RT = 1.113 min, m/z = 618.5 $[M+H]^+$.

Step 6. 5'-(4-Fluorophenyl)-3'-isopropyl-N-(4-(4-methylpiperazin-1-yl)phenyl)-1H,3'H-2,4'-biimidazole-4-carboxamide **4**. To a solution of 5'-(4-fluorophenyl)-3'-isopropyl-N-(4-(4-methylpiperazin-1-yl)phenyl)-1-((2-(trimethylsilyl)ethoxy)methyl)-1H,3'H-2,4'-biimidazole-4-carboxamide **10–7** (50 mg, 80.93 μ mol, 1.0 eq) in DCM (1 mL) was added TFA (1.54 g, 13.51 mmol, 1 mL, 166.9 eq) at 20 °C. The mixture was stirred at 20 °C for 6 h. Then $NH_3 \cdot H_2O$ (0.4 mL) was added. The mixture was concentrated under reduced pressure to afford a residue. The residue was purified by prep-HPLC (column: Shim-pack C18 150*25*10um; mobile phase: [water(0.225%FA)-ACN]; $B\%$: 5%–25%, 10 min) to afford 5'-(4-fluorophenyl)-3'-isopropyl-N-(4-(4-methylpiperazin-1-yl)phenyl)-1H,3'H-2,4'-biimidazole-4-carboxamide **4** (30.88 mg, 50.92 μ mol, 62.92% yield, 99.2% purity, TFA) as white solid. 1H NMR: (400 MHz, $DMSO-d_6$), δ = 13.06 (br s, 1H), 9.76 (s, 1H), 8.07 (s, 1H), 7.99 (d, J = 2.2 Hz, 1H), 7.70 (d, J = 9.0 Hz, 2H), 7.42–7.35 (m, 2H), 7.17–7.10 (m, 2H), 6.94 (d, J = 9.0 Hz, 2H), 4.28–4.18 (m, 1H), 3.25–3.20 (m, 4H), 2.94 (br d, J = 2.2 Hz, 4H), 2.57 (br s, 3H), 1.39 (d, J = 6.6 Hz, 6H). ^{19}F NMR: (400 MHz, $DMSO-d_6$), δ = –73.45 (s, 3F), –115.58 (s, 1F). LC-MS: $[M+H]^+$ calculated for $C_{27}H_{30}FN_7O$: 506.25; found: 488.26. Other analogs **10a–10o** could be prepared through a similar method (Supporting Information).

Synthesis of 11a. **Step 1.** 4-(3,4-Difluorophenyl)-1H-imidazole **11–3a**. To a solution of 4-bromo-1H-imidazole **11–1** (2.00 g, 13.6 mmol, 1.0 eq) and 3,4-difluorophenylboronic acid **11–2a** (4.30 g, 27.2 mmol, 2.0 eq) in dioxane (20 mL) and H_2O (4 mL) was added CsF (6.20 g, 40.82 mmol, 3.0 eq), K_2CO_3 (3.76 g, 27.22 mmol, 2.0 eq) and $Pd(PPh_3)_4$ (2.36 g, 2.04 mmol, 0.15 eq). The mixture was stirred at 100 °C under N_2 atmosphere for 16 h. The reaction mixture was poured into H_2O (150 mL) and extracted with EA (100 mL \times 2). The combined organic layer was adjusted to pH = 2 with 2 N HCl solution, then the aqueous layer was adjusted to pH = 8 with Na_2CO_3 and extracted with EA (100 mL \times 3), the combined organic layer was washed with brine (100 mL), dried over Na_2SO_4 , filtered and concentrated. The crude product was used for the next step directly. 4-(3,4-Difluorophenyl)-1H-imidazole **11–3a** (6.3 g, 34.97 mmol, 64.25% yield) was obtained as yellow solid. LC-MS: RT = 0.840 min, m/z = 181.1 $[M+H]^+$.

Step 2. 4-(3,4-Difluorophenyl)-1-isopropyl-1H-imidazole **11–4a**. To a solution of 4-(3,4-difluorophenyl)-1H-imidazole **11–3a** (9.50 g, 52.7 mmol, 1.0 eq) in DMF (100 mL) was added NaH (4.22 g, 105 mmol, 60% purity, 2.0 equiv) at 0 °C and stirred at 0 °C for 30 min. Then 2-bromopropane (7.78 g, 63.3 mmol, 5.94 mL, 1.2 eq) was added at 0 °C and stirred at 80 °C for 12 h. The mixture was poured into a saturated NH_4Cl solution (120 mL), and then extracted with ethyl acetate (100 mL \times 2). The combined organic layer was washed with brine (150 mL), dried over Na_2SO_4 , filtered, and concentrated under reduced pressure to give a residue. The crude product was used for the next step directly without purification. 4-(3,4-Difluorophenyl)-1-isopropyl-1H-imidazole **11–4a** (11 g, 49.50 mmol, 93.86% yield) was obtained as yellow oil. LC-MS: RT = 0.542 min, m/z = 223.1 $[M+H]^+$.

Step 3. 4-(3,4-Difluorophenyl)-5-iodo-1-isopropyl-1H-imidazole **11–5a**. To a solution of 4-(3,4-difluorophenyl)-1-isopropyl-1H-imidazole **11–4a** (11.0 g, 49.5 mmol, 1.0 eq) in DCM (110 mL) was added NIS (33.4 g, 148 mmol, 3.0 eq) and TFA (1.69 g, 14.9 mmol, 1.10

mL, 0.30 eq). The mixture was stirred at 25 °C for 12 h. The mixture was poured into an aq. Na₂SO₃ solution (100 mL × 3) and extracted with DCM (100 mL × 3). The organic phase was washed with brine (100 mL), dried over anhydrous Na₂SO₄, and concentrated in vacuum to give a residue. The residue was purified by column chromatography (SiO₂, PE/EA = 10:1 to 5:1). 4-(3,4-Difluorophenyl)-5-iodo-1-isopropyl-1H-imidazole **11-5a** (15 g, 39.64 mmol, 80.09% yield) was obtained as yellow solid. LC-MS: RT = 0.759 min, *m/z* = 349.0 [M + H⁺].

Step 4. 4-(3,4-Difluorophenyl)-1-isopropyl-5-(tributylstannyl)-1H-imidazole 11-6a. To a solution of 4-(3,4-difluorophenyl)-5-iodo-1-isopropyl-1H-imidazole **11-5a** (2.00 g, 5.74 mmol, 1.0 eq) in THF (30 mL) was added *n*-BuLi (2.5 M, 2.99 mL, 1.3 eq) and Sn(Bu)₃Cl (2.81 g, 8.62 mmol, 2.32 mL, 1.5 eq) slowed at −70 °C. The mixture was stirred at −70 °C for 30 min and then stirred at −40 °C for another 30 min. The mixture was poured into an aqueous KF (200 mL) and saturated NH₄Cl solution (150 mL), and then extracted with DCM (200 mL × 3). The combined organic layer was washed with brine (200 mL), dried over Na₂SO₄, filtered, and concentrated under reduced pressure to give a residue. The residue was purified by column chromatography (SiO₂, PE/EA = 10:1 to 5:1 to 3:1 to 1:1, P: Rf = 0.2). 4-(3,4-Difluorophenyl)-1-isopropyl-5-(tributylstannyl)-1H-imidazole **11-6a** (4 g, 6.96 mmol, 30.30% yield, 89% purity) was obtained as yellow oil. LC-MS: RT = 1.002 min, *m/z* = 513.2 [M + H⁺].

Step 5. Ethyl 5'-(3,4-Difluorophenyl)-3'-isopropyl-1-((2-(trimethylsilyl)ethoxy)methyl)-1H,3'H-2,4'-biimidazole-4-carboxylate 11-10a. To a solution of 4-(3,4-difluorophenyl)-1-isopropyl-5-(tributylstannyl)-1H-imidazole **11-6a** (300 mg, 522 μmol, 89% purity, 1.0 eq) and ethyl 2-bromo-1-((2-(trimethylsilyl)ethoxy)methyl)-1H-imidazole-4-carboxylate **11-9** (218.89 mg, 626.67 μmol, 1.2 eq) in toluene (3 mL) was added cataCXium A Pd G2 (107 mg, 160 μmol, 3.06e^{−1} eq). The mixture was stirred at 110 °C for 12 h. The mixture was concentrated under reduced pressure to give a residue. The residue was purified by column chromatography (SiO₂, PE/EA = 10:1 to 2:1, P: Rf = 0.3). Ethyl 5'-(3,4-difluorophenyl)-3'-isopropyl-1-((2-(trimethylsilyl)ethoxy)methyl)-1H,3'H-2,4'-biimidazole-4-carboxylate **11-10a** (600 mg, 880.52 μmol, 42.15% yield) was obtained as yellow oil. LC-MS: RT = 0.957 min, *m/z* = 491.4 [M + H⁺].

Step 6. 5'-(3,4-Difluorophenyl)-3'-isopropyl-1-((2-(trimethylsilyl)ethoxy)methyl)-1H,3'H-2,4'-biimidazole-4-carboxylic Acid 11-11a. To a solution of ethyl 5'-(3,4-difluorophenyl)-3'-isopropyl-1-((2-(trimethylsilyl)ethoxy)methyl)-1H,3'H-2,4'-biimidazole-4-carboxylate **11-10a** (600 mg, 880 μmol, 72% purity, 1.0 eq) in THF (6 mL) was added LiOH (105 mg, 4.40 mmol, 5.0 eq) in H₂O (2 mL). The mixture was stirred at 25 °C for 2 h. The reaction mixture was adjusted to pH = 2 with HCl/dioxane (4N) solution and concentrated under reduced pressure to give a residue. The residue was purified by prep-HPLC (column: Phenomenex luna C18 150 × 40 mm × 15 μm; mobile phase: [water (0.225%FA)-ACN]; B%: 35%–65%, 10 min). 5'-(3,4-Difluorophenyl)-3'-isopropyl-1-((2-(trimethylsilyl)ethoxy)methyl)-1H,3'H-2,4'-biimidazole-4-carboxylic acid **11-11a** (250 mg, 524.25 μmol, 59.54% yield) was obtained as yellow solid. LC-MS: RT = 0.878 min, *m/z* = 463.4 [M + H⁺].

Step 7. 5'-(3,4-Difluorophenyl)-3'-isopropyl-N-(4-(4-methylpiperazin-1-yl)phenyl)-1-((2-(trimethylsilyl)ethoxy)methyl)-1H,3'H-2,4'-biimidazole-4-carboxamide 11-12a. To a solution of 5'-(3,4-difluorophenyl)-3'-isopropyl-1-((2-(trimethylsilyl)ethoxy)methyl)-1H,3'H-2,4'-biimidazole-4-carboxylic acid **11-11a** (100 mg, 216 μmol, 1.0 eq) and 4-(4-methylpiperazin-1-yl)aniline (49.6 mg, 259 μmol, 1.2 eq) in DMF (2 mL) was added HATU (164.40 mg, 432.37 μmol, 2.0 eq) and DIEA (83.82 mg, 648.56 μmol, 112.97 μL, 3.0 eq). The mixture was stirred at 25 °C for 2 h. The mixture was poured into H₂O (10 mL) and extracted with EA (10 mL × 3). The organic phase was washed with brine (20 mL), dried over anhydrous Na₂SO₄, and concentrated under reduced pressure to give a residue. The crude product was used for the next step without purification. 5'-(3,4-Difluorophenyl)-3'-isopropyl-N-(4-(4-methylpiperazin-1-yl)phenyl)-1-((2-(trimethylsilyl)ethoxy)methyl)-1H,3'H-2,4'-biimidazole-4-carboxamide **11-12a** (120 mg, crude) was obtained as yellow oil. LC-MS: RT = 0.874 min, *m/z* = 436.4 [M + H⁺].

Step 8. 5'-(3,4-Difluorophenyl)-3'-isopropyl-N-(4-(4-methylpiperazin-1-yl)phenyl)-1H,3'H-2,4'-biimidazole-4-carboxamide 11a. To a solution of 5'-(3,4-difluorophenyl)-3'-isopropyl-N-(4-(4-methylpiperazin-1-yl)phenyl)-1-((2-(trimethylsilyl)ethoxy)methyl)-1H,3'H-2,4'-biimidazole-4-carboxamide **11-12a** (120 mg, 188 μmol, 1.0 eq) in DCM (0.5 mL) was added TFA (3.08 g, 27.0 mmol, 2 mL, 143 eq). The mixture was stirred at 25 °C for 2 h. Another batch of TFA (1.54 g, 13.51 mmol, 1 mL, 71.6 eq) was added to the reaction and was stirred at 25 °C for another 2 h. The mixture was adjusted to pH = 7 with an aqueous NaHCO₃ solution and extracted with EA (10 mL × 3). The organic phase was washed with brine (20 mL), dried over anhydrous Na₂SO₄, and concentrated under reduced pressure to give a residue. The residue was purified by prep-HPLC (column: Phenomenex Gemini-NX C18 75 × 30 mm × 3 μm; mobile phase: [water (10 mM NH₄HCO₃)-ACN]; B%: 20%–50%, 8 min). 5'-(3,4-Difluorophenyl)-3'-isopropyl-N-(4-(4-methylpiperazin-1-yl)phenyl)-1H,3'H-2,4'-biimidazole-4-carboxamide **11a** (23.9 mg, 38.12 μmol, 20.20% yield, TFA salt) was obtained as off-white solid. ¹H NMR: (400 MHz, DMSO-*d*₆), δ = 9.73 (s, 1H), 8.10 (s, 1H), 8.01 (s, 1H), 7.66 (br d, *J* = 8.8 Hz, 2H), 7.42–7.31 (m, 2H), 7.08 (br d, *J* = 1.6 Hz, 1H), 6.90 (br d, *J* = 8.8 Hz, 2H), 4.30–4.16 (m, 1H), 3.09 (br d, *J* = 4.4 Hz, 4H), 2.52 (br s, 2H), 2.24 (s, 3H), 2.07 (s, 2H), 1.39 (d, *J* = 6.8 Hz, 6H). LC-MS: [M + H⁺] calculated for C₂₇H₂₉F₂N₇O: 506.25; found: 506.40. Other analogs **11b** and **11c** could be prepared through a similar method (Supporting Information).

Chemistry42 Modeling. The structural model of the TNIK kinase domain built on the SAX9 TNIK cocrystal structure and structure-based drug-design workflow implemented in the Chemistry42 platform were used to generate a library of virtual structures. Pocket and Pharmacophore Reward modules were used for scoring produced designs and navigating the generative process. The TNIK ATP-binding site was selected as a target-binding pocket. The generated structures had to match at least a two-point pharmacophore hypothesis that consisted of the hydrogen bond acceptor forming an H-bond with the NH of Cys108 of the hinge region and hydrophobic center occupying the space near the gatekeeper Met105. In addition to the assessment by Pocket and Pharmacophore modules, the engine penalized structures that violated the predefined ranges of the physicochemical properties (logP, molecular weight, number of hydrogen bond donors, hydrogen bond acceptor, topological polar surface area, number of atoms, number of rotatable bonds, number of aromatic rings), medicinal chemistry filters and the synthetic accessibility score threshold.

TNIK Inhibition Radiometric Assay. Compounds were screened against selected kinases using Eurofins' standard KinaseProfiler assays. The assay involved adding the 50x stock of the test compound to the assay well, followed by the introduction of a reaction mix containing the enzyme and substrate. The reaction commenced with the addition of ATP at the selected concentration, with no preincubation of the compound with the enzyme/substrate mix. Detailed assay protocols for each individual kinase are accessible on the Eurofins Web site or in the accompanying protocol document.

TNIK(h) was incubated with 8 mM MOPS pH 7.0, 0.2 mM EDTA, 250 μM RLGRDKYKTLRQIRQ, 10 mM MgAcetate and [gamma-33P-ATP] (specific activity and concentration as required). The reaction was initiated by the addition of the Mg/ATP mix. After incubation for 40 min at room temperature, the reaction was stopped by the addition of phosphoric acid to a concentration of 0.5%. Ten μL of the reaction was then spotted onto a P30 filter mat and washed four times for 4 min in 0.425% phosphoric acid and once in methanol prior to drying and scintillation counting. Data analysis utilized custom-built in-house software. Results were expressed as kinase activity remaining, calculated as a percentage of the DMSO control. IC₅₀ determination involved analyzing the data using XLfit version 5.3, fitting sigmoidal dose–response curves.

LX-2 Cell Toxicity and Fibrosis Assay. Compounds were diluted to nine concentrations by 3-fold serial dilution with DMSO. These dilutions were used to treat LX-2 cells, with top concentrations at 100 μM for a tested compound, and 250 μM for Sorafenib. CellTiter-Glo Luminescent Cell Viability Assay was used to determine cell viability after treatment. The diluted compounds were transferred into a 96-well

plate in duplicate. The culture medium was prepared with DMEM, 2% FBS, and 1% P/S. The medium was removed from a confluent layer of LX-2 cells, and cells were trypsinized, centrifuged, resuspended in fresh medium, and counted. 5000 cells/well were seeded into 96-well plates. Controls included medium without cells and compound-free wells. The final DMSO concentration was 0.5%. Cells were incubated for 72 h at 37 °C with 5% CO₂. After 72 h, 50 μ L of the medium was reserved, and 50 μ L of CellTiter-Glo reagent was added. Luminescence was measured to calculate cell viability (%). CC50 was calculated from cell viability data using GraphPad Prism software.

For the fibrosis assay, test compounds were diluted to eight concentrations. LX-2 cells were treated with these dilutions for 30 min before being stimulated with TGF- β for 48 h. Cells were then lysed, and protein concentrations were determined. Immunoblotting was performed with adjusted protein concentrations. Blots were visualized, and data were quantified using ImageQuant TL. IC₅₀ values for fibrosis markers were calculated using GraphPad Prism software.

FRET Assay. 100 nL of a compound solution was transferred into an assay plate. Five μ L of TNIK and Ser/Thr 7 peptide mixture was dispensed into assay plate columns 2 to 23 and wells A24–H24. For negative controls, 5 μ L of 0% phosphorylation solution was dispensed into wells A1–H1 and I24–P24. For positive controls, 5 μ L of 100% phosphorylation solution was added to wells I1–P1. The assay plate was then spun at 1,000 rpm for 60 s. Then the plate was spun at 1,000 rpm for 60 s and incubated at 23 °C for 15 min. Following this, 5 μ L of ATP solution was added to all wells, the plate was spun again, and incubated for 60 min. A detection reagent was then added, the plate was spun once more, incubated for another 60 min, and read using an Envision plate reader. Finally, the data were analyzed to calculate IC₅₀ values.

Kinetic Solubility. Test and control compounds (10 μ L of 10 mM in DMSO) were added to the lower chambers of Whatman Mini-Uniprep vials. Next, 490 μ L of 50 mM phosphate buffer (pH 7.4) was added to the same chamber. The samples were vortexed for 2 min and then shaken at room temperature for 24 h at 800 rpm. After shaking, the vials were centrifuged for 20 min at 4000 rpm and compressed to prepare the filtrate. The filtrate was then injected into a UPLC system to determine the concentration of the compound using a standard curve.

LogD Assay. Test and control compounds (2 μ L of 10 mM DMSO stock solution) were aliquoted into tubes in duplicate. To each tube, 149 μ L of phosphate buffer (PB, pH 1.8, 2.5, 4.5, 7.4, 9.5, 11.0, and 12.0) saturated with 1-octanol, and 149 μ L of 1-octanol saturated with the same PB were added. The tubes were mixed vigorously for 2 min and then shaken for 1 h at 800 rpm at room temperature. After centrifugation at 4000 rpm for 5 min, buffer and 1-octanol layer samples were aliquoted. These samples were diluted and detected using LC-MS/MS without calibration curves. LogD values were calculated using the following equation:

$$\log D_{\text{Octanol/Buffer}} = \frac{\log_{10} \frac{\text{mean buffer layer peak area ratio} \times \text{buffer layer dilution factor}}{\text{mean octanol layer peak area ratio} \times \text{octanol layer dilution factor}}}$$

Microsomal Metabolic Stability Assay. Liver microsomes were diluted to 0.56 mg/mL in 100 mM phosphate buffer. Microsome working solutions (445 μ L, 0.56 mg/mL) were transferred into prewarmed incubation plates T60 and NCF60 and preincubated for 10 min at 37 °C with constant shaking. In the blank plate, 54 μ L liver microsomes, 6 μ L NADPH cofactor, and 180 μ L quenching solution were added. A 5 μ L compound working solution (100 μ M) was added to the incubation plates (T60 and NCF60) containing microsomes and mixed thoroughly. For the NCF60 plate, 50 μ L of buffer was added and mixed thoroughly. The plate was incubated at 37 °C for 60 min while shaking. In the quenching plate T0, 180 μ L quenching solution and 6 μ L NADPH cofactor were added. The plate was chilled to prevent evaporation. For the T60 plate, the mixture was thoroughly mixed, and 54 μ L was immediately transferred to the quenching plate for the 0 min time point. Then, 44 μ L NADPH cofactor was added to the incubation plate (T60), which was incubated at 37 °C for 60 min while shaking. At 5, 10, 20, 30, and 60 min, 180 μ L quenching solution was added to

quenching plates, mixed once, and 60 μ L samples were serially transferred from the T60 plate per time point to quenching plates. For NCF60, the sample was mixed once, and 60 μ L was transferred from the NCF60 incubation to the quenching plate at the 60 min time point. All sampling plates were shaken for 10 min, then centrifuged at 4000 rpm for 20 min at 4 °C. An 80 μ L supernatant was transferred into 240 μ L HPLC water and mixed with a plate shaker for 10 min. Each bioanalysis plate was sealed and shaken for 10 min prior to LC-MS/MS analysis.

First-order kinetics was used to calculate half-life and intrinsic clearance. Half-life is derived from the elimination rate constant (k_e). Intrinsic clearance was determined from k_e , adjusting for liver weight.

Plasma Protein Binding. The dialysis device was assembled according to the manufacturer's instructions. To load the device, 200 μ L of loading plasma containing 0.1, 1, and 10 μ M of a tested compound or 5 μ M of phenacetin, quinidine, and warfarin were transferred in triplicate to the donor side of each dialysis well, and 350 μ L of Dialysis Buffer was added to the receiver side. The plate was sealed and rotated at approximately 150 rpm in a humidified incubator with 5% CO₂ at 37 °C for 4 h. For T0 samples, 50 μ L of loading plasma with the test compounds was transferred in triplicate to a 96-well plate, matched with blank buffer to a final volume of 100 μ L, and mixed with 300 μ L stop solution, then stored at 4 °C. T4 samples were prepared similarly and incubated for 4 h. After dialysis, 50 μ L samples were taken from both sides of the device and matched with opposite blank buffer or plasma to 100 μ L. All samples were processed by protein precipitation for LC-MS/MS analysis. Concentrations of a tested compound were quantitatively determined by LC-MS/MS after protein precipitation. The peak area ratios of analyte/internal standard were used to semiquantitatively determine the concentrations of control compounds (phenacetin, quinidine, and warfarin) by LC-MS/MS.

CYP450 Isoforms Inhibition. Detailed information can be found in the [Supporting Information](#).

Ames Test. For the mutagenicity assay, 2 mL molten top agar was mixed with 0.5 mL phosphate buffer/S9 mix, 0.1 mL dose formulation, and 0.1 mL bacterial culture, then overlaid on bottom agar plates. The plates were incubated at 37 \pm 1 °C for 48–72 h. Triplicate plates were prepared for test compound, negative and positive controls. For the collection of results, plates were examined for background lawn and precipitation, and revertant colonies were manually counted. The dose-dependent increase in revertant colonies for the test compound was assessed.

hERG Inhibition Assay. hERG-expressing HEK293 cells were prepared, cultured, and resuspended in a low-calcium extracellular solution suitable for patch-clamp recording. The cell suspension was loaded into the QPatch instrument, and the automated cell capture, seal formation, and whole-cell configuration steps were initiated. A series of voltage clamp steps were applied to record baseline hERG currents, followed by the addition of test compound at 10 μ M in two replicates to assess its inhibitory effects on hERG channel activity. The resulting current traces were analyzed to determine the percent inhibition of hERG currents by a tested compound.

PXR Activation. A 6.4 mL cell recovery medium (CRM-PXR) was added to 1 tube of the frozen PXR reporter cells, resulting in a final volume of 7 mL per tube. The cells were warmed in a 37 °C water bath for 5–10 min. 200 μ L of cell suspension was added to each well, ensuring no cells were added to the LCMA blank wells. The seeded cells were then returned to a humidified CO₂ (5%) incubator at 37 °C for 4–6 h. Test compound, vehicle control, and positive control dosing solutions were prepared and warmed in a 37 °C water bath. After incubation, the cells were retrieved, and the medium was aspirated from each well. 200 μ L of the warm dosing solution was added to each well in triplicate, and 200 μ L vehicle control dosing solution to the blank wells. The seeded cells were returned to a humidified CO₂ (5%) incubator at 37 °C for 22–24 h. After that, the cells were rinsed once with 200 μ L LCMA buffer at room temperature. 50 μ L of LCMA reagent was added to each well, and the plate was tilted side-to-side 2–3 times before incubating in the dark for 15 min at room temperature. The LDR reagent was prepared by adding 1 vial of detection substrate (2 mL) to 1 vial of detection buffer (2 mL). At the end of the 15 min incubation, the LCMA reagent was aspirated, and 100 μ L LDR was added to each well,

incubating for at least 5 min. After at least 5 min of incubation following the addition of LDR, the luminescence (RLU) was read using a SpectraMax M4 plate reader with a 500 ms reading time per well.

SAFETYscan assay. Each assay followed a Eurofins SAFETYscan standardized procedure. The assays were performed utilizing the PathHunter enzyme fragment complementation (EFC) technology, FLIPR-based cellular screening assays, KINOMEScan kinase binding, ion channels, transporters, nuclear hormone receptor, calcium mobilization, GPCR cAMP assays, and a variety of enzymatic assays. Compound activity was analyzed using the CBIS data analysis suite.

PK in Mice. In this study, CD-1 mice were once dosed with a tested compound at a dose of 30 mg/kg orally or 3 mg/kg intravenously. The intravenous administration dose volume was 5 mL/kg. A validated LC-MS/MS method was used to determine the concentration of a tested compound in CD-1 mice plasma. The lower limit of detection (LLOQ) was 0.5 ng/mL. The noncompartment model of WinNonlin software (version 8.1) was used to calculate the main pharmacokinetic parameters of a tested compound.

This study was conducted in compliance with the “Guide for the Care and Use of Laboratory Animals” (2011) issued by the National Research Council, USA, “Laboratory Animal Administration” (revised in 2017) issued by the State Science and Technology Committee, People’s Republic of China, and “Laboratory Animal Administration Regulations” (2008) issued by the Jiangsu Laboratory Animal Administration Office. The protocol, amendment(s), and procedures involving the care and use of animals in the study were reviewed and approved by the Institutional Animal Care and Use Committee (IACUC) of the test facility. IACUC number:2021–303.

PK in Dogs. Beagle Dogs were once dosed with a tested compound at a dose of 10 mg/kg orally or 1 mg/kg intravenously. The intravenous administration dose volume was 1 mL/kg. A validated LC-MS/MS method was used to determine the concentration of a tested compound in Beagle Dog plasma. The lower limit of quantitation (LLOQ) was 0.5 ng/mL. The noncompartment model of WinNonlin software (version 8.1) was used to calculate the main pharmacokinetic parameters of a tested compound.

This study was conducted in compliance with the “Guide for the Care and Use of Laboratory Animals” (2011) issued by the National Research Council, USA, “Laboratory Animal Administration” (revised in 2017) issued by the State Science and Technology Committee, People’s Republic of China, and “Laboratory Animal Administration Regulations” (2008) issued by the Jiangsu Laboratory Animal Administration Office. The protocol, amendment(s), and procedures involving the care and use of animals in the study were reviewed and approved by the Institutional Animal Care and Use Committee (IACUC) of the test facility. IACUC number:2021–305.

CCL4-Induced Liver Fibrosis in Mice. This experiment was performed by the contract research organization Physiogenex (France). CCl₄ (ref#289116 from Sigma-Aldrich - Batch # SHBK7) was administered to 8-week old male C57BL6/J mice by i.p. (10% CCl₄ in corn oil, 3.5 μ L/g body weight) twice weekly for 4 weeks. After the first 2 weeks post CCl₄ stimulation, mice were randomized based on blood ALT, ALT levels as well as body weight, then were treated with compound 4 or vehicle (0.5% methylcellulose) orally twice a day for 2 weeks. At the end of the study, mice were euthanized and then exsanguinated with saline before liver collection. Liver samples were dissected from the left lateral lobe to prepare FFPE samples for Sirius red staining and pathologic analysis.

For pathology analysis for fibrosis, whole-section histomorphometric measurements of the Sirius Red-positive area were conducted through computer-assisted image analysis. These measurements were obtained using Visiopharm software (version VIS 2020.08, Denmark). Evaluations for morphometric analysis were carried out on virtual whole sections at 20 \times magnification. An algorithm was developed to measure Sirius Red in liver-stained sections using the Bayesian linear segmentation tool within a software package. This algorithm was fine-tuned through training on a subset of sections from 5 animals. Major histological artifacts, large vascular and portal structures, were automatically identified and excluded from the area of interest (AOI) or detected positive areas.

The NAFLD activity score (NAS)⁴⁰ was generated using an analysis of H&E and Sirius Red staining, and was based on the scorings evaluated for hepatocellular steatosis, liver inflammation, lobular fibrosis, and hepatocyte ballooning.

■ ASSOCIATED CONTENT

Supporting Information

The Supporting Information is available free of charge at <https://pubs.acs.org/doi/10.1021/acs.jmedchem.4c01580>.

Additional experimental details and methods; X-ray data collection and refinement; synthesis and characterization of the final compounds (PDF)

Molecular formula strings (CSV)

PDB ID Code: 8ZML, the cocrystal structure of the TNIK kinase domain and compound 4; Structural model of the TNIK kinase domain with an alternative conformation of gatekeeper Met105 (PDB)

■ AUTHOR INFORMATION

Corresponding Author

Vladimir Aladinskiy – *Insilico Medicine AI Ltd., Abu Dhabi 145748, United Arab Emirates*; orcid.org/0000-0002-3976-3991; Email: vladimir@insilicomedicine.com

Authors

Chris Kruse – *Insilico Medicine Hong Kong Ltd., Pak Shek Kok, New Territories 999077, Hong Kong*

Luoheng Qin – *Insilico Medicine Shanghai Ltd., Shanghai 200120, China*

Eugene Babin – *Insilico Medicine AI Ltd., Abu Dhabi 145748, United Arab Emirates*

Yaya Fan – *Insilico Medicine Shanghai Ltd., Shanghai 200120, China*

Georgiy Andreev – *Insilico Medicine AI Ltd., Abu Dhabi 145748, United Arab Emirates*

Heng Zhao – *Insilico Medicine Shanghai Ltd., Shanghai 200120, China*

Yanyun Fu – *Insilico Medicine Shanghai Ltd., Shanghai 200120, China*

Man Zhang – *Insilico Medicine Shanghai Ltd., Shanghai 200120, China*

Yan Ivanenkov – *Insilico Medicine Hong Kong Ltd., Pak Shek Kok, New Territories 999077, Hong Kong*; orcid.org/0000-0002-8968-0879

Alex Aliper – *Insilico Medicine AI Ltd., Abu Dhabi 145748, United Arab Emirates; Insilico Medicine Hong Kong Ltd., Pak Shek Kok, New Territories 999077, Hong Kong*; orcid.org/0000-0002-4363-0710

Alex Zhavoronkov – *Insilico Medicine AI Ltd., Abu Dhabi 145748, United Arab Emirates; Insilico Medicine Hong Kong Ltd., Pak Shek Kok, New Territories 999077, Hong Kong; Insilico Medicine Canada Inc, Montréal, Québec H3B 4W8, Canada*; orcid.org/0000-0001-7067-8966

Feng Ren – *Insilico Medicine AI Ltd., Abu Dhabi 145748, United Arab Emirates; Insilico Medicine Shanghai Ltd., Shanghai 200120, China*; orcid.org/0000-0001-9157-9182

Complete contact information is available at:

<https://pubs.acs.org/10.1021/acs.jmedchem.4c01580>

Notes

The authors declare the following competing financial interest(s): All authors work for Insilico Medicine, a commercial artificial intelligence company.

■ ABBREVIATIONS

AI, artificial intelligence; ALK4, anaplastic lymphoma kinase 4; CHRM1, muscarinic acetylcholine receptor M1; CK1 δ , casein kinase I isoform delta; $Cl_{int(mic)}$, intrinsic clearance in microsome; COL1, collagen type 1; CRC, colorectal cancer; ECM, extracellular matrix; EGFR, epidermal growth factor receptor; HLM, human liver microsomes; HMS, hepatocyte metabolic stability; HSC, hepatic stellate cells; JNK, c-Jun N-terminal kinase; KS, kinetic solubility; LCK, lymphocyte-specific protein tyrosine kinase; LSCC, lung squamous cell carcinoma; MLM, mouse liver microsomes; PDGFR α , platelet-derived growth factor receptor α ; SEM, trimethylsilylethoxymethyl; SPR, surface plasmon resonance; TAZ, transcriptional coactivator with PDZ-binding motif; TCF4, T-cell factor 4; TGF- β , transforming growth factor beta; TGF β R1, transforming growth factor beta receptor 1; TNBC, triple-negative breast cancer; TNiK, Traf2- and Nck-interacting kinase; VEGFR2, vascular endothelial growth factor receptor 2; YAS, yes-associated protein; α -SMA, alpha-smooth muscle actin

■ REFERENCES

- (1) Hu, G.; Huang, N.; Zhang, J.; Zhang, D.; Wang, S.; Zhang, Y.; Wang, L.; Du, Y.; Kuang, S.; Ma, K.; Zhu, H.; Xu, N.; Liu, M. LKB1 Loss Promotes Colorectal Cancer Cell Metastasis through Regulating TNiK Expression and Actin Cytoskeleton Remodeling. *Molecular Carcinogenesis* **2023**, 62 (11), 1659–1672.
- (2) Takahashi, C.; Kondo, S.; Sadaoka, K.; Ishizuka, S.; Noguchi, K.; Kato, Y.; Sugimoto, Y. Effect of TNiK Upregulation on JQ1-Resistant Human Colorectal Cancer HCT116 Cells. *Biochem. Biophys. Res. Commun.* **2020**, 530 (1), 230–234.
- (3) Zhou, K.; Cheong, J. E.; Krishnaji, S. T.; Ghalali, A.; Fu, H.; Sui, L.; Alix-Panabières, C.; Cayrefourcq, L.; Bielenberg, D.; Sun, L.; Zetter, B. Inhibition of Wnt Signaling in Colon Cancer Cells via an Oral Drug That Facilitates TNiK Degradation. *Molecular Cancer Therapeutics* **2023**, 22 (1), 25–36.
- (4) Masuda, M.; Sawa, M.; Yamada, T. Therapeutic Targets in the Wnt Signaling Pathway: Feasibility of Targeting TNiK in Colorectal Cancer. *Pharmacology & Therapeutics* **2015**, 156, 1–9.
- (5) Kim, J.; Oh, J.; Peterson, H. M.; Carlson, J. C. T.; Pittet, M. J.; Weissleder, R. TNiK Inhibition Has Dual Synergistic Effects on Tumor and Associated Immune Cells. *Advanced Biology* **2022**, 6 (8), 2200030.
- (6) Torres-Ayuso, P.; An, E.; Nyswaner, K. M.; Bensen, R. C.; Ritt, D. A.; Specht, S. I.; Das, S.; Andresson, T.; Cachau, R. E.; Liang, R. J.; Ries, A. L.; Robinson, C. M.; Difilippantonio, S.; Gouker, B.; Bassel, L.; Karim, B. O.; Miller, C. J.; Turk, B. E.; Morrison, D. K.; Brognard, J. TNiK Is a Therapeutic Target in Lung Squamous Cell Carcinoma and Regulates FAK Activation through Merlin. *Cancer Discovery* **2021**, 11 (6), 1411–1423.
- (7) Sato, K.; Padgaonkar, A. A.; Baker, S. J.; Cosenza, S. C.; Rechakoblit, O.; Subbaiah, D. R. C. V.; Domingo-Domenech, J.; Bartkowski, A.; Port, E. R.; Aggarwal, A. K.; Ramana Reddy, M. V.; Irie, H. Y.; Reddy, E. P. Simultaneous CK2/TNiK/DYRK1 Inhibition by 108600 Suppresses Triple Negative Breast Cancer Stem Cells and Chemotherapy-Resistant Disease. *Nat. Commun.* **2021**, 12 (1), 4671.
- (8) Puleo, N.; Cusato, M.; Carvette, D.; Husdon, C.; DiFeo, A. Abstract 1679: Unraveling the Function of TRAF2 and NCK Interacting Kinase (TNiK) in High-Grade Serous Ovarian Cancer. *Cancer Res.* **2023**, 83 (7_Supplement), 1679–1679.
- (9) Li, J.; Lan, L.; Xu, Y.; Liu, S.; Liu, M.; Hu, G.; Wu, G.; Zhao, Y.; Shi, J.; Wang, J.; Sun, Y.; Wang, Z.; Zhao, R. Expression Analysis of TRAF2- and NCK-interacting Protein Kinase (TNiK) and Phosphorylated TNiK in Papillary Thyroid Carcinoma. *Oncol. Lett.* **2023**, 26 (1), 310.
- (10) Yang, Y.-F.; Yu, B.; Zhang, X.-X.; Zhu, Y.-H. Identification of TNiK as a Novel Potential Drug Target in Thyroid Cancer Based on Protein Druggability Prediction. *Medicine* **2021**, 100 (16), No. e25541.
- (11) Yi, D.; Zhang, D.; Zeng, Z.; Zhang, S.; Li, M.; Zhang, Y. MicroRNA-144–3p Represses the Growth and EMT of Thyroid Cancer via the E2F2/TNiK Axis in Cells and Male BALB/c Nude Mice. *Endocrinology* **2022**, 163 (7), bqac071.
- (12) Sekita, T.; Yamada, T.; Kobayashi, E.; Yoshida, A.; Hirozane, T.; Kawai, A.; Uno, Y.; Moriyama, H.; Sawa, M.; Nagakawa, Y.; Tsuchida, A.; Matsumoto, M.; Nakamura, M.; Nakayama, R.; Masuda, M. Feasibility of Targeting Traf2-and-Nck-Interacting Kinase in Synovial Sarcoma. *Cancers* **2020**, 12 (5), 1258.
- (13) Masuda, M.; Uno, Y.; Ohbayashi, N.; Ohata, H.; Mimata, A.; Kukimoto-Niino, M.; Moriyama, H.; Kashimoto, S.; Inoue, T.; Goto, N.; Okamoto, K.; Shirouzu, M.; Sawa, M.; Yamada, T. TNiK Inhibition Abrogates Colorectal Cancer Stemness. *Nat. Commun.* **2016**, 7 (1), 12586.
- (14) Li, Y.; Zhang, L.; Yang, R.; Qiao, Z.; Wu, M.; Huang, C.; Tian, C.; Luo, X.; Yang, W.; Zhang, Y.; Li, L.; Yang, S. Discovery of 3,4-Dihydrobenzo[*f*][1,4]Oxazepin-5(2*H*)-One Derivatives as a New Class of Selective TNiK Inhibitors and Evaluation of Their Anti-Colorectal Cancer Effects. *J. Med. Chem.* **2022**, 65 (3), 1786–1807.
- (15) Ho, K.-K.; Parnell, K. M.; Yuan, Y.; Xu, Y.; Kultgen, S. G.; Hamblin, S.; Hendrickson, T. F.; Luo, B.; Foulks, J. M.; McCullar, M. V.; Kanner, S. B. Discovery of 4-Phenyl-2-Phenylaminopyridine Based TNiK Inhibitors. *Bioorg. Med. Chem. Lett.* **2013**, 23 (2), 569–573.
- (16) Fang, Y.; Tian, J.; Fan, Y.; Cao, P. Latest Progress on the Molecular Mechanisms of Idiopathic Pulmonary Fibrosis. *Mol. Biol. Rep.* **2020**, 47 (12), 9811–9820.
- (17) Trachalaki, A.; Sultana, N.; Wells, A. U. An Update on Current and Emerging Drug Treatments for Idiopathic Pulmonary Fibrosis. *Expert Opinion on Pharmacotherapy* **2023**, 24 (10), 1125–1142.
- (18) Kamy, P.; Ozerov, I. V.; Pun, F. W.; Tretina, K.; Fokina, T.; Chen, S.; Naumov, V.; Long, X.; Lin, S.; Korzinkin, M.; Polykovskiy, D.; Aliper, A.; Ren, F.; Zhavoronkov, A. PandaOmics: An AI-Driven Platform for Therapeutic Target and Biomarker Discovery. *J. Chem. Inf. Model.* **2024**, 64 (10), 3961–3969.
- (19) Ren, F.; Aliper, A.; Chen, J.; Zhao, H.; Rao, S.; Kuppe, C.; Ozerov, I. V.; Zhang, M.; Witte, K.; Kruse, C.; Aladinskiy, V.; Ivanenkov, Y.; Polykovskiy, D.; Fu, Y.; Babin, E.; Qiao, J.; Liang, X.; Mou, Z.; Wang, H.; Pun, F. W.; Ayuso, P. T.; Veviorskiy, A.; Song, D.; Liu, S.; Zhang, B.; Naumov, V.; Ding, X.; Kukhareenko, A.; Izumchenko, E.; Zhavoronkov, A. A Small-Molecule TNiK Inhibitor Targets Fibrosis in Preclinical and Clinical Models. *Nat. Biotechnol.* **2024**.
- (20) Zhou, D.; Huang, W.; Wei, J.; Zhang, J.; Liu, Z.; Ji, R.; Ge, S.; Xiao, M.; Fan, Y.; Lu, C. RelB Promotes Liver Fibrosis via Inducing the Release of Injury-associated Inflammatory Cytokines. *J. Cellular Molecular Med.* **2020**, 24 (11), 6008–6014.
- (21) Shkoda, A.; Town, J. A.; Griesse, J.; Romio, M.; Sarioglu, H.; Knöfel, T.; Giehler, F.; Kieser, A. The Germinal Center Kinase TNiK Is Required for Canonical NF- κ B and JNK Signaling in B-Cells by the EBV Oncoprotein LMP1 and the CD40 Receptor. *PLoS Biol.* **2012**, 10 (8), No. e1001376.
- (22) Caba, M. P.; Komiyama, N. H.; Nithianantharajah, J.; Kopanitsa, M. V.; Indersmitten, T.; Skene, N. G.; Tuck, E. J.; Fricker, D. G.; Elsegood, K. A.; Stanford, L. E.; Afinowi, N. O.; Saksida, L. M.; Bussey, T. J.; O'Dell, T. J.; Grant, S. G. N. TNiK Is Required for Postsynaptic and Nuclear Signaling Pathways and Cognitive Function. *J. Neurosci.* **2012**, 32 (40), 13987–13999.
- (23) Popmihajlov, Z.; Sutherland, D. J.; Horan, G. S.; Ghosh, A.; Lynch, D. A.; Noble, P. W.; Richeldi, L.; Reiss, T. F.; Greenberg, S. CC-90001, a c-Jun N-Terminal Kinase (JNK) Inhibitor, in Patients with Pulmonary Fibrosis: Design of a Phase 2, Randomised, Placebo-Controlled Trial. *BMJ. Open Res.* **2022**, 9 (1), No. e001060.
- (24) Li, Q.; Nirala, N. K.; Chen, H.; Nie, Y.; Wang, W.; Zhang, B.; Czech, M. P.; Wang, Q.; Xu, L.; Mao, J.; Ip, Y. T. The Misshapen Subfamily of Ste20 Kinases Regulate Proliferation in the Aging

Mammalian Intestinal Epithelium. *Journal Cellular Physiology* **2019**, *234* (12), 21925–21936.

(25) Kim, J.; Moon, S.-H.; Kim, B. T.; Chae, C. H.; Lee, J. Y.; Kim, S. H. A Novel Aminothiazole KY-05009 with Potential to Inhibit Traf2- and Nck-Interacting Kinase (TNIK) Attenuates TGF- β 1-Mediated Epithelial-to-Mesenchymal Transition in Human Lung Adenocarcinoma A549 Cells. *PLoS One* **2014**, *9* (10), No. e110180.

(26) Buchl, S. C.; Hanquier, Z.; Haak, A. J.; Thomason, Y. M.; Huebert, R. C.; Shah, V. H.; Maiers, J. L. Traf2 and NCK Interacting Kinase Is a Critical Regulator of Procollagen I Trafficking and Hepatic Fibrogenesis in Mice. *Hepatology* **2022**, *6* (3), 593–609.

(27) Pham, T. C. P.; Dollet, L.; Ali, M. S.; Raun, S. H.; Møller, L. L. V.; Jafari, A.; Ditzel, N.; Andersen, N. R.; Fritzen, A. M.; Gerhart-Hines, Z.; Kiens, B.; Suomalainen, A.; Simpson, S. J.; Salling Olsen, M.; Kieser, A.; Schjerling, P.; Nieminen, A. I.; Richter, E. A.; Havula, E.; Sylow, L. TNIK Is a Conserved Regulator of Glucose and Lipid Metabolism in Obesity. *Sci. Adv.* **2023**, *9* (32), No. ead7119.

(28) Pun, F. W.; Leung, G. H. D.; Leung, H. W.; Liu, B. H. M.; Long, X.; Ozerov, I. V.; Wang, J.; Ren, F.; Aliper, A.; Izumchenko, E.; Moskalev, A.; De Magalhães, J. P.; Zhavoronkov, A. Hallmarks of Aging-Based Dual-Purpose Disease and Age-Associated Targets Predicted Using PandaOmics AI-Powered Discovery Engine. *Aging* **2022**, *14* (6), 2475–2506.

(29) Ewald, C. Y.; Pulous, F. E.; Lok, S. W. Y.; Pun, F. W.; Aliper, A.; Ren, F.; Zhavoronkov, A. TNIK's Emerging Role in Cancer, Metabolism, and Age-Related Diseases. *Trends Pharmacol. Sci.* **2024**, *45* (6), 478–489.

(30) Zuccotto, F.; Ardini, E.; Casale, E.; Angiolini, M. Through the "Gatekeeper Door": Exploiting the Active Kinase Conformation. *J. Med. Chem.* **2010**, *53* (7), 2681–2694.

(31) Scapin, G.; Patel, S. B.; Lisnock, J.; Becker, J. W.; LoGrasso, P. V. The Structure of JNK3 in Complex with Small Molecule Inhibitors. *Chemistry & Biology* **2003**, *10* (8), 705–712.

(32) Peifer, C.; Abadleh, M.; Bischof, J.; Hauser, D.; Schattel, V.; Hirner, H.; Knippschild, U.; Laufer, S. 3,4-Diaryl-Isoxazoles and -Imidazoles as Potent Dual Inhibitors of P38 α Mitogen Activated Protein Kinase and Casein Kinase 1 δ . *J. Med. Chem.* **2009**, *52* (23), 7618–7630.

(33) Du, Y.; Jamasb, A. R.; Guo, J.; Fu, T.; Harris, C.; Wang, Y.; Duan, C.; Liò, P.; Schwaller, P.; Blundell, T. L. Machine Learning-Aided Generative Molecular Design. *Nat. Mach. Intell.* **2024**, *6* (6), 589–604.

(34) Zhavoronkov, A.; Ivanenkov, Y. A.; Aliper, A.; Veselov, M. S.; Aladinskiy, V. A.; Aladinskaya, A. V.; Terentiev, V. A.; Polykovskiy, D. A.; Kuznetsov, M. D.; Asadulaev, A.; Volkov, Y.; Zholus, A.; Shayakhmetov, R. R.; Zhebrak, A.; Minaeva, L. I.; Zagribelnyy, B. A.; Lee, L. H.; Soll, R.; Madge, D.; Xing, L.; Guo, T.; Aspuru-Guzik, A. Deep Learning Enables Rapid Identification of Potent DDR1 Kinase Inhibitors. *Nat. Biotechnol.* **2019**, *37* (9), 1038–1040.

(35) Ivanenkov, Y. A.; Polykovskiy, D.; Bezrukov, D.; Zagribelnyy, B.; Aladinskiy, V.; Kamya, P.; Aliper, A.; Ren, F.; Zhavoronkov, A. Chemistry42: An AI-Driven Platform for Molecular Design and Optimization. *J. Chem. Inf. Model.* **2023**, *63* (3), 695–701.

(36) Beno, B. R.; Yeung, K.-S.; Bartberger, M. D.; Pennington, L. D.; Meanwell, N. A. A Survey of the Role of Noncovalent Sulfur Interactions in Drug Design. *J. Med. Chem.* **2015**, *58* (11), 4383–4438.

(37) Thompson, K.; Maltby, J.; Fallowfield, J.; McAulay, M.; Millward-Sadler, H.; Sheron, N. Interleukin-10 Expression and Function in Experimental Murine Liver Inflammation and Fibrosis. *Hepatology* **1998**, *28* (6), 1597–1606.

(38) Thaher, B. A.; Koch, P.; Schattel, V.; Laufer, S. Role of the Hydrogen Bonding Heteroatom–Lys53 Interaction between the P38 α Mitogen-Activated Protein (MAP) Kinase and Pyridinyl-Substituted 5-Membered Heterocyclic Ring Inhibitors. *J. Med. Chem.* **2009**, *52* (8), 2613–2617.

(39) Velaparthi, U.; Darne, C. P.; Warriar, J.; Liu, P.; Rahaman, H.; Augustine-Rauch, K.; Parrish, K.; Yang, Z.; Swanson, J.; Brown, J.; Dhar, G.; Anandam, A.; Holenarsipur, V. K.; Palanisamy, K.; Wautlet, B. S.; Fereshteh, M. P.; Lippy, J.; Tebben, A. J.; Sherif, S.; Ruzanov, M.; Yan, C.; Gupta, A.; Gupta, A. K.; Vetrichelvan, M.; Mathur, A.; Gelman,

M.; Singh, R.; Kinsella, T.; Murtaza, A.; Fargnoli, J.; Vite, G.; Borzilleri, R. M. Discovery of BMS-986260, a Potent, Selective, and Orally Bioavailable TGF β /R1 Inhibitor as an Immuno-Oncology Agent. *ACS Med. Chem. Lett.* **2020**, *11* (2), 172–178.

(40) Kleiner, D. E.; Brunt, E. M.; Van Natta, M.; Behling, C.; Contos, M. J.; Cummings, O. W.; Ferrell, L. D.; Liu, Y.-C.; Torbenson, M. S.; Unalp-Arida, A.; Yeh, M.; McCullough, A. J.; Sanyal, A. J. Nonalcoholic Steatohepatitis Clinical Research Network. Design and Validation of a Histological Scoring System for Nonalcoholic Fatty Liver Disease. *Hepatology* **2005**, *41* (6), 1313–1321.